LOCAL DENSITY OF STATES OF AN ISOLATED VORTEX IN THE QUASICLASSICAL LIMIT

A Thesis

Presented to

The Faculty of Graduate Studies

of

The University of Guelph

by

WILLIAM CHI-FAI WONG

In partial fulfilment of requirements

for the degree of

Master of Science

August, 1998

Canada

ABSTRACT

LOCAL DENSITY OF STATES OF AN ISOLATED VORTEX

IN THE QUASICLASSICAL LIMIT

William Chi-Fai Wong   Advisor:
University of Guelph. 1998   Professor E.J. Nicol

It is well known that when a magnetic field is applied to so-called type II superconductors. magnetic flux is able to penetrate in quantized amounts by forming cylindrical domains known as vortices. Within a vortex core. the superconductivity is suppressed. and single-particle excitations are observed. In this thesis. we calculate the local density of states for an isolated vortex using a variety of order parameters. The calculations are performed within the framework of the quasiclassical Eilenberger theory. We find that the states within the core do not represent those of the normal region. Instead. the distribution of the local density of states is characterized by the order parameter.

Acknowledgements

I would like to begin by thanking my supervisor. Professor Elisabeth Nicol, for her guidance and encouragement throughout this research. She introduced me to the field of superconductivity, created a learning environment to study this topic, and provided me with the freedom to pursue other areas of interest. Also, I wish to thank my supervisory committee, Professors Bernie Nickel and Don Sullivan, along with Dr. Ilya Vekhter, for their insightful comments and suggestions.

Many people have been a great influence on my life over the course of this degree, and I would like to express my gratitude to all of them. In particular, I want to take this opportunity to thank my friends and housemates Jeff Broderick, Yasuhiro Mori, Sandy Roberts, and Marcus Wilker. Because of them, home was always a fun place to be. A special thanks goes to Patricia Robertson for her wonderful advice and friendship. And finally, thank-you to all of the undergraduates in first year, for providing some meaning to this work.

I want to thank my parents and my sister Barbara for all of their encouragement. And last but not least, I would like to thank Anka Pawelczyk. There are no words to describe her warmth and support over the years.

Contents

List of Figures

Chapter 1

Superconductivity

Certain materials, when cooled below a critical temperature T_c, undergo a transition into the superconducting phase, which is characterized by zero dc electrical resistance and perfect diamagnetism. Since its discovery in 1911, superconductivity has been observed in a variety of materials, such as metals, alloys, ceramics and organic compounds, thereby creating an exciting area of study for both experimental and theoretical physicists.

A fundamental problem in superconductivity is to determine the symmetry of a superconductor's energy gap. One possible tool for extracting this information is the scanning tunneling microscope, which can directly image the local density of states around a vortex in a type II superconductor. As we shall see, the local density of states reflects the symmetry of the order parameter.

However, before turning our attention to vortices and their bound states, let us first review the history of superconductivity. Since the following section is limited to introducing some essential terminology, the reader may also wish to consult Refs. [1], [2], and [3].

1.1 History of superconductivity

In 1908. H. Kamerlingh Onnes[4] succeeded in liquefying helium. thus initiating the field of low temperature physics. Three years later. he observed that the dc resistance of mercury dropped to zero at $4.15K$. At any temperature T below this critical temperature. the normal resistance could be restored by applying a minimum magnetic field $H_c(T)$.

Several years passed before the second distinguishing feature of superconductivity was observed. In 1933. W. Hans Meissner and Robert Ochsenfeld[5] found that when a superconductor is cooled below its transition temperature in a magnetic field. it excludes the magnetic flux. This phenomena. known as the Meissner effect. distinguishes a superconductor from a perfect conductor. as the latter would lock in the flux according to Lenz's law. The superconductor's ability to exclude any magnetic flux is a property known as perfect diamagnetism.

1.1.1 Phenomenological theories

A number of phenomenological theories were proposed well before the formation of a full quantum mechanical treatment. The London theory. introduced in 1933 by the brothers Fritz and Heinz London[6], noted that an external magnetic field decays exponentially in the bulk of a superconductor over a distance known as the *penetration depth* λ. In 1953. A.B. Pippard[7] extended the London theory by defining another length scale. known as the *coherence length* ξ, to account for nonlocal interactions of the electron assembly. Pippard's coherence length measures the distance in which a significant change could occur in the superconductor's electronic structure[1].

---

[1]In the microscopic theory, the spatial extent of the BCS wavefunction is interpreted as the coherence length.

Meanwhile, a thermodynamic model was proposed by V.L. Ginzburg and L.D. Landau[8] in 1950. They assumed that the current in the superconducting state was carried by "super electrons" with effective mass m^*, charge e^*, and density n_s^*. It was later shown that these variables are related to their electron counterparts m, e, and n as follows:

$$\begin{aligned} m^* &= 2m. \\ e^* &= \pm 2e. \\ n_s^* &= \tfrac{1}{2}n. \end{aligned}$$

(1.1)

At T_c, the super electrons start to form, and increase in number as the temperature decreases. Thus, their density n_s^* is a measure of the order that exists within the superconducting state. Accordingly, the Ginzburg-Landau (GL) theory defines a complex *order parameter* $\psi(\mathbf{r})$, whose magnitude $|\psi(\mathbf{r})|$ is related to the super electron density.

$$|\psi(\mathbf{r})| = \sqrt{n_s^*(\mathbf{r})}.$$

(1.2)

Above T_c, the order parameter is zero, and its magnitude increases smoothly as T is reduced below T_c in zero field. The GL equations are obtained by minimizing the free energy density, expanded in powers of the order parameter, near T_c.

One result from the GL theory is that the interphase surface energy density between the normal and superconducting phases σ_{ns} is dependent on a dimensionless parameter called κ. To explain the Meissner effect, a very large positive energy is required, which results when $\kappa \ll 1$.

Ginzburg and Landau noted, but did not pursue, that for $\kappa > 1/\sqrt{2}$, σ_{ns} became negative. This was later recognized as the defining difference between type I and type II superconductors. In type I superconductors, a sharp transition between the superconducting and normal state is observed when $H_c(T)$ is applied. For type II

superconductors. the Meissner effect is observed when the applied field strength is below a lower critical field $H_{c1}(T)$. For field strengths above $H_{c1}(T)$, it becomes energetically favourable for the superconductor to allow some magnetic flux to pass through by creating normal regions. This mixed state exists until the field strength reaches an upper critical field $H_{c2}(T)$, in which the normal state is restored. In 1957, A.A. Abrikosov[9] proposed that the magnetic flux in the mixed state penetrates the superconductor in discrete amounts by forming domains called *vortices*. Section §1.4 discusses these vortices in further detail.

1.1.2 Microscopic theory of superconductivity

In 1957, Bardeen, Cooper, and Schrieffer[10] developed a microscopic theory of superconductivity, which is commonly called *BCS theory*. Section §1.2 outlines some of the properties of this theory.

The original BCS work was based on a variational solution of the Schrödinger equation for a gas of electrons with a pairing interaction. The BCS theory may also be described using a field theory technique known as Green's functions. Using this method, L.P. Gor'kov[11] developed the Green's function equations for superconductivity in 1958. The quasiclassical limit was expressed by Eilenberger[12], and independently by Larkin and Ovchinnikov[13], in 1968.

1.1.3 High-T_c superconductors

Interest in high temperature superconductors started in 1986, with K.A. Müller's and J.G. Bednorz's[14] discovery of superconductivity in lanthanum and barium copper oxides ($Ba_xLa_{5-x}Cu_5O_y$) at temperatures below $35K$. Although still below the boiling point of liquid nitrogen ($77K$), this discovery focused attention on the copper

oxide compounds. Within a year, the yttrium-barium systems ($YBa_2Cu_3O_{7-\delta}$) were discovered with transition temperatures in the low $90K$'s. Within another year, the T_c rose to $110K$ with the discovery of $Bi_2Sr_2Ca_2Cu_3O_{10}$ superconductors, and then to $125K$ for $Tl_2Ba_2Ca_2Cu_3O_{10}$. In 1993, the mercury compounds ($HgBa_2Ca_2Cu_3O_{8+\delta}$) boosted the transition temperature to $133K$. Under extremely high pressure[2], T_c's in excess of $150K$ have been observed.

1.2   BCS theory

The simplest model for superconductivity is that of a gas of electrons interacting with each other through some two-particle interaction. In 1956, Cooper[15] considered the problem of two electrons which lie above the Fermi sphere. He demonstrated that if the electrons could be paired by some interaction that was attractive, then a bound state could form.

Although any mechanism leading to a net attractive interaction would also lead to a superconducting state. Cooper argued that a plausible mechanism arises from the motion of the ions, or phonons. (Experimental evidence of the direct involvement of phonons in the superconducting transition is provided by the isotope effect, in which the critical temperature is dependent on the ionic mass.) Even though the direct electrostatic interaction is repulsive, the ionic motion can overscreen the Coulomb interaction. This yields a net attraction between electrons in the Cooper pair. The pair is also prevented from occupying states below k_F, due to the Pauli exclusion principle of the remaining electrons in the Fermi sphere.

In 1957, Bardeen, Cooper, and Schrieffer[10] extended the pairing idea such that all electrons within $\hbar\omega_D$ of ϵ_F participated in one of the bound states (where the

---

[2]Pressures on the order of 25-30 GPa.

5

Debye frequency ω_D is a measure of the maximum phonon frequency. and ϵ_F is the Fermi energy). In the BCS theory. the ground state wavefunction of N conduction electrons is the product of $\frac{N}{2}$ paired bound-state wavefunctions. The product is antisymmetrized to incorporate the exclusion principle. The antisymmetry prevents a one-electron level from being doubly occupied. but places no such restrictions on a two-electron level. Thus. the pair of electrons can behave statistically like bosons. As well. the paired wavefunctions are taken to be singlet states (the triplet state leads to magnetic properties not observed in conventional superconductors).

The BCS theory provides a microscopic interpretation of the phenomenological parameters. The spatial extent of the BCS wavefunction is known as the coherence length ξ_0. A simple estimate of ξ_0 is given by:

$$\xi_0 \sim \frac{\hbar v_F}{\Delta} \sim \frac{\epsilon_F}{k_F \Delta}. \tag{1.3}$$

where Δ is the energy gap for a homogeneous and isotropic superconductor (see Section §1.2.2). In typical low-T_c superconductors. ϵ_F is 10^3 times Δ. and k_F is of the order 10^8 cm^{-1}. giving a coherence length of 10^3Å.

1.2.1 BCS order parameter

The mathematics of BCS theory is best described by second quantized notation. where the fermion creation operator $\hat{\psi}_\sigma^\dagger(\mathbf{x})$ "creates" a fermion with spin $\sigma = \pm\frac{1}{2}$ at a position $\mathbf{x}$. A similar annihilation operator $\hat{\psi}_\sigma(\mathbf{x})$ removes a fermion with spin σ at a position $\mathbf{x}$. These operators have the following anticommutation relations:

$$\begin{aligned}
\{\hat{\psi}_\alpha(\mathbf{x}), \hat{\psi}_\beta^\dagger(\mathbf{x}')\} &= \delta_{\alpha\beta}\delta(\mathbf{x} - \mathbf{x}'), \\
\{\hat{\psi}_\alpha(\mathbf{x}), \hat{\psi}_\beta(\mathbf{x}')\} &= 0
\end{aligned} \tag{1.4}$$

Using these operators. the superconducting order parameter[3] is naturally defined as:

$$F_{\alpha J}^{\dagger}(\mathbf{x}, \mathbf{x}') = \left\langle \hat{\psi}_{\alpha}^{\dagger}(\mathbf{x}) \hat{\psi}_{J}^{\dagger}(\mathbf{x}') \right\rangle. \tag{1.5}$$

along with its complex conjugate:

$$F_{\alpha J}(\mathbf{x}, \mathbf{x}') = \left\langle \hat{\psi}_{\alpha}(\mathbf{x}) \hat{\psi}_{J}(\mathbf{x}') \right\rangle. \tag{1.6}$$

where the angular brackets imply a thermal average taken over all states. The anticommutation relations indicate that the order parameter is antisymmetric under exchange of coordinates and spin:

$$F_{\alpha J}(\mathbf{x}, \mathbf{x}') = -F_{J\alpha}(\mathbf{x}', \mathbf{x}). \tag{1.7}$$

For a spin singlet state. separation of Eq. (1.7) into its spin and coordinate components gives:

$$F_{\alpha J}(\mathbf{x}, \mathbf{x}') = \chi_{\alpha J} F(\mathbf{x}, \mathbf{x}'). \tag{1.8}$$

where $\chi_{\alpha J} = -\chi_{J\alpha}$. It follows that the space part of the order parameter is symmetric since the overall order parameter is antisymmetric:

$$F(\mathbf{x}, \mathbf{x}') = F(\mathbf{x}', \mathbf{x}). \tag{1.9}$$

Another useful operator to define is the translation operator $\hat{T}(\mathbf{a})$. which when acting on a field operator $\hat{\psi}_{\sigma}(\mathbf{x})$, gives:

$$\hat{T}(\mathbf{a}) \hat{\psi}_{\sigma}(\mathbf{x}) \hat{T}^{-1}(\mathbf{a}) = \hat{\psi}_{\sigma}(\mathbf{x} + \mathbf{a}) \tag{1.10}$$

Thus. applying the translation operator to the order parameter in the absence of a magnetic field gives:

$$F(\mathbf{x}, \mathbf{x}') = F(\mathbf{x} + \mathbf{a}, \mathbf{x}' + \mathbf{a}). \tag{1.11}$$

---

[3]In the theory of phase transitions. an order parameter is a quantity that vanishes in the disordered (or symmetric, or high-temperature) phase, while in the ordered phase it has a non-zero value.

Since **a** is an arbitrary translation. Eq. (1.11) implies that the spatial order parameter is only dependent on the relative position:

$$F(\mathbf{x}, \mathbf{x}') = F(\mathbf{x} - \mathbf{x}'). \tag{1.12}$$

1.2.2 BCS gap equation

The next step is to introduce[4] a *gap function*:

$$\Delta(\mathbf{x} - \mathbf{x}') = F(\mathbf{x} - \mathbf{x}')V(\mathbf{x} - \mathbf{x}'), \tag{1.13}$$

where $V(\mathbf{x} - \mathbf{x}')$ is the interaction potential between electrons.

It is convienent to express $F(\mathbf{x} - \mathbf{x}')$, $V(\mathbf{x} - \mathbf{x}')$ and $\Delta(\mathbf{x} - \mathbf{x}')$ in terms of their Fourier transforms:

$$F(\mathbf{x} - \mathbf{x}') = \frac{1}{\Omega} \sum_{\mathbf{k}} e^{i\mathbf{k}(\mathbf{x}-\mathbf{x}')} F_{\mathbf{k}}, \tag{1.14}$$

$$V(\mathbf{x} - \mathbf{x}') = \frac{1}{\Omega} \sum_{\mathbf{k}} e^{i\mathbf{k}(\mathbf{x}-\mathbf{x}')} V_{\mathbf{k}}. \tag{1.15}$$

$$\Delta(\mathbf{x} - \mathbf{x}') = \frac{1}{\Omega} \sum_{\mathbf{k}} e^{i\mathbf{k}(\mathbf{x}-\mathbf{x}')} \Delta_{\mathbf{k}}. \tag{1.16}$$

where Ω is the volume of the system. Convolution gives the relationship between $F_{\mathbf{k}}$, $V_{\mathbf{k}}$ and $\Delta_{\mathbf{k}}$ to be:

$$\Delta_{\mathbf{k}} = \frac{1}{\Omega} \sum_{\mathbf{k}'} V_{\mathbf{k}-\mathbf{k}'} F_{\mathbf{k}'}. \tag{1.17}$$

Using Eqs. (1.5) - (1.17), a Hamiltonian for an electron system can be diagonalized by a transformation known as the Bogoliubov transformation. The details are not presented here, and may be found in Refs. [1] and [2].

---

[4]Although not presented here, the motivation for such an introduction arises from solving the potential energy component of the Hamiltonian, where the product $F_{\alpha\beta}(\mathbf{x}, \mathbf{x}')V(\mathbf{x} - \mathbf{x}')$ appears frequently. The gap equation also has a physical meaning, which we will soon see.

Without further discussion. we state that the finite temperature solution to the energy gap is defined self-consistently as:

$$\Delta_{\mathbf{k}}(T) = \frac{1}{\Omega} \sum_{\mathbf{k}'} V_{\mathbf{k},\mathbf{k}'} \Delta_{\mathbf{k}'}(T) \left(\frac{1 - 2f(E_{\mathbf{k}'})}{2E_{\mathbf{k}'}} \right). \tag{1.18}$$

$$E_{\mathbf{k}} = \left(\epsilon_{\mathbf{k}}^2 + |\Delta_{\mathbf{k}}(T)|^2 \right)^{1/2} \tag{1.19}$$

where $f(E)$ is the Fermi-Dirac distribution function. and $\epsilon_{\mathbf{k}}$ is the energy of a state relative to the Fermi surface. In the original BCS model. the pairing interaction $V_{\mathbf{k},\mathbf{k}'} = V_0$ is a non-zero positive constant for a range of energies $|\epsilon_{\mathbf{k}}| < \hbar\omega_D$ and $|\epsilon_{\mathbf{k}'}| < \hbar\omega_D$.

When $\Delta_{\mathbf{k}}$ has non-trivial solutions. the excitation spectrum (1.19) has a minimum value of $\Delta_{\mathbf{k}}$. In other words. single-particle excitations must supply at least a minimum gap energy to excite the superconducting condensate.

In the literature. commonly encountered order parameters include: the s-wave. which has an energy gap that is finite and single-valued for all k directions. and the $d_{x^2-y^2}$-wave. which has a gap that vanishes whenever $k_x^2 - k_y^2 = 0$. The $d_{x^2-y^2}$-wave is a likely order parameter for the high-T_c copper oxides.

1.3 Scope of the thesis

We focus our attention on the following situation: Within a vortex of a type II superconductor. the superconductivity is suppressed. The vortex can be viewed as a quantum mechanical potential well, whereby single-particle excitations can form bound states. We study these states using the quasiclassical Eilenberger theory. The quasiclassical approach applies to superconductors which have a coherence length much longer than the inverse Fermi momentum, $k_F\xi_0 \gg 1$. Previous theoretical work

9

describing the excitations in an isolated vortex based on the quasiclassical theory has been put forth by Klein (s-wave)[19], Gygi and Schlüter (s-wave)[20, 21], Schopohl and Maki ($d_{x^2-y^2}$-wave)[22], and Hayashi *et al.*(anisotropic s-wave)[23, 24].

Using a scheme similar to that of Schopohl and Maki[22] as well as Hayashi *et al.*[23], we calculate the local density of states around an isolated vortex. First, we reproduce the above authors results for the s-wave, $d_{x^2-y^2}$-wave (or d-wave for short), and anisotropic s-wave gaps. Then, we continue with a study of the following four order parameters:

- $d_{x^2-y^2} + i\alpha d_{xy}$-wave ($d + i\alpha d$).

- g-wave.

- $s + \alpha d_{x^2-y^2}$ ($s + \alpha d$).

- and $d_{x^2-y^2} + \alpha s$-wave ($d + \alpha s$).

The motivation of this thesis stems from the following experimental and theoretical situations: (1) Direct imaging of the bound states, or local density of states, is now possible with STM spectroscopy. Future STM experiments on different superconductors, including the high-T_c copper oxides, are anticipated. (2) A parameterization of the Eilenberger equations has been developed which greatly reduces the numerical calculations. Remarkably, the quasiclassical Green's functions can be calculated by solving an initial value problem of an ordinary differential equation.

We conclude this chapter by discussing vortices in more detail. Chapter 2 will describe the theory of the Eilenberger equations and how it is applied to our work. Chapter 3 is dedicated to presenting the results of our calculations. Finally, in Chapter 4, a summary and conclusion of the work done in this thesis will be given.

1.4 Vortices in type II superconductors

In type II superconductors. the normal and superconducting states coexist over a range of magnetic field strengths. The normal regions in the mixed state form tubes. or vortices. which extend the length of the superconductor. The order parameter vanishes at the center of the vortex. and increases on the length scale ξ_0. This defines a region known as the vortex core. The magnetic field is largest in the core. and decays over a length scale λ. Circulating currents flow around the core. screening the field from the bulk of the superconductor. Each vortex encloses one quanta of magnetic flux $hc/2e$ (see Figure 1.1).

1.4.1 Experimental studies of vortices

The electronic structure of vortices may be studied using scanning tunneling microscopy (STM) experiments. The scanning tunneling microscope consists of a probe. or tip. which can be positioned with atomic resolution. The tip scans the surface of the superconductor at a fixed height. The tunneling current through the tip is measured as a function of voltage: the differential conductance dI/dV is directly proportional to the local density of states (LDOS).

In 1989. Hess *et al.*[16. 17. 18] examined the vortex structure of 2H-NbSe$_2$. a layered hexagonal superconducting compound. which is thought to have an *s*-wave order parameter. They found a zero-bias voltage peak in the measured differential conductance at the vortex center. which splits into two (ie: a positive and negative bias voltage peak) as one moves farther away from the core center. As well, the LDOS was star shaped. with the orientation of the star being dependent on the bias voltage.

11

Specifically. the characteristic features of the LDOS observed in $NbSe_2$ are summarized in detail as follows. when a magnetic field H is applied perpendicular to the hexagonal plane[23]: (1) The LDOS for quasiparticle excitations has a sixfold star shape centered at the vortex center. (2) The orientation of this star depends on the energy. At zero bias. a ray of the star extends away from the x axis (or a axis) in the hexagonal plane of $NbSe_2$. Upon increasing the bias voltage. the star rotates by 30°. (3) In the intermediate bias voltage. a ray splits into a pair of nearly parallel rays. keeping its direction fixed. (4) In the spectral evolution which crosses the vortex center. there exist inner peaks in addition to the outer peaks which evolve from the zero bias peak at the vortex center into the bulk BCS-like gap edges far from the vortex. The inner peaks vary with the angle of the direction in which the spectral evolution is taken.
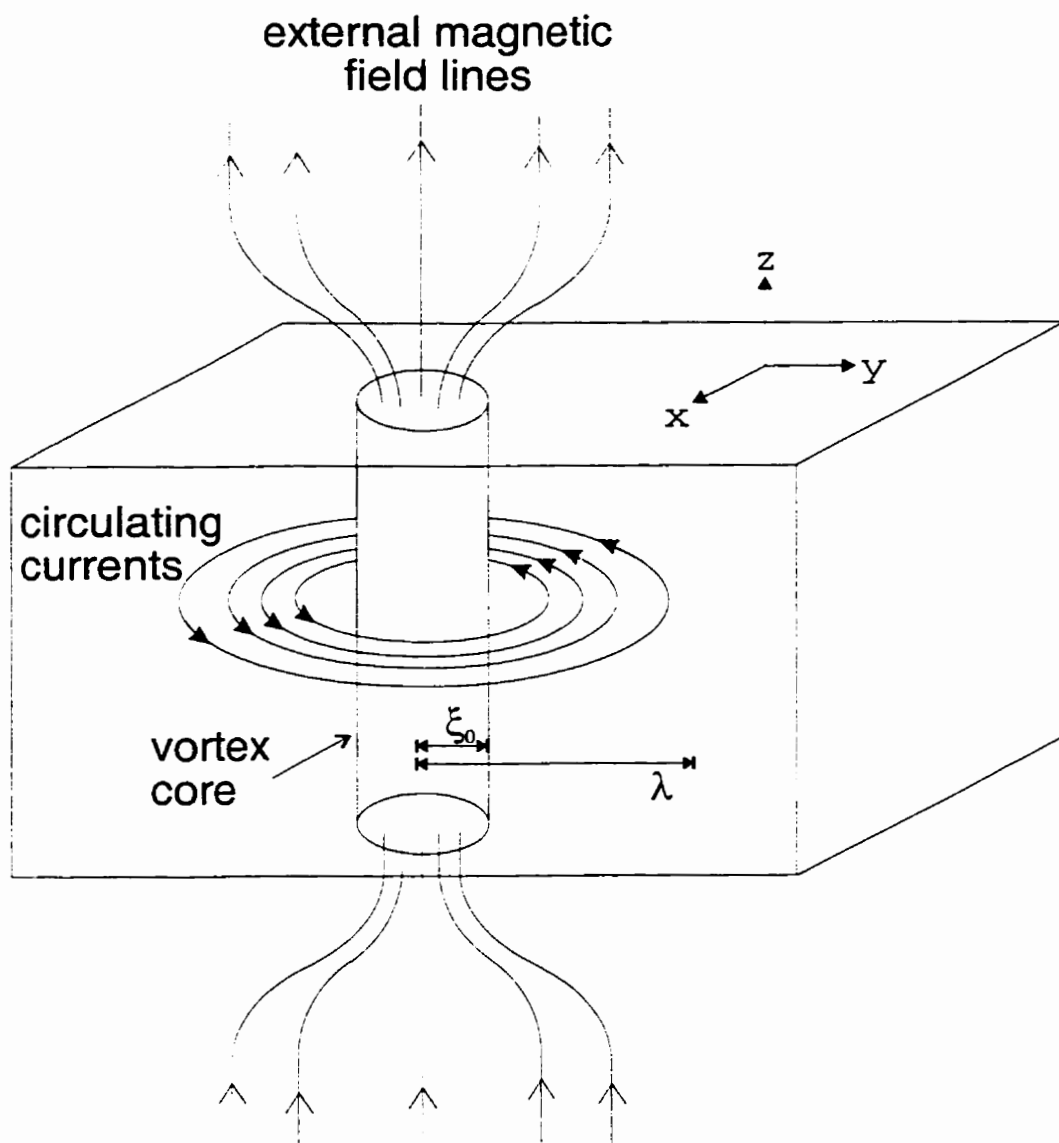
Figure 1.1: Sketch of a vortex.

Chapter 2

Theoretical Methods

The foundation for almost all theoretical work on type II superconductivity has been laid by Gor'kov[11], with the formulation of a set of equations for four Green's functions supplemented by two self-consistent equations for the gap equation Δ and vector potential A. However, information on the order of k_F^{-1} contained in the Gor'kov equations is unnecessary to describe the STM results. The length scale of interest for most superconductivity experiments is on the order of the BCS coherence length ξ_0.

The quasiclassical formulation, derived by Eilenberger [12] and independently by Larkin and Ovchinnikov [13], simplify the Gor'kov equations by solving for what is called the ξ-integrated form of the Green's functions. These integrated Green's functions still contain much more information than is needed in most cases, yet the resulting equations benefit from a reduction in complexity and provide a promising starting point for numerical calculations[12].

In this chapter, Section §2.1 provides a brief overview of Gor'kov's and Eilenberger's methods for describing superconductivity with Green's functions. For a full mathematical description, refer to [25]. In Section §2.2, the quasiclassical formalism is presented. Sections §2.3 describes a parameterization which reduces the Eilenberger

equation to a initial value problem of an ordinary differential equation. Using this method. the local density of states around a vortex core is calculated.

2.1 Green's function method

The concept of a 'propagator' or 'Green's function' was originally developed in the study of quantum electrodynamics. but has since been applied to many areas in physics. It provides a useful set of mathematical techniques for deriving physical results with minimum use of auxiliary and unobservable functions. In principle the wavefunction of a quantum state contains all the physical information about the state. The propagator is a closely related function. which represents the correlation between the states of the system at different times[26].

The original BCS derivation demonstrated that superconductivity cannot be obtained by a perturbation expansion in powers of the effective potential. As a result. a single propagator G cannot solve a model Hamiltonian with pairing interactions. However. Gor'kov showed how the Green's function may be calculated by introducing new anomalous propagators. F and $F^\dagger$. which destroy or create a Cooper pair in the superconducting ground state. The matrix propagator $\hat{G}$ is a compact representation of these Green's functions:

$$\hat{G} = \begin{pmatrix} G & F \\ F^\dagger & -G \end{pmatrix}.$$

(2.1)

The matrix propagator satisfies a Dyson equation together with a prescription for calculating the self energy:

$$(\hat{G}_0^{-1} - \hat{\Sigma})\hat{G} = \hat{1}.$$

(2.2)

$$\hat{\Sigma} = \hat{\Sigma}(\hat{G}).$$

(2.3)

Here $\hat{G}_0$ is the free-electron propagator.

In the quasiclassical formalism. the Green's functions appear in the ξ_k-integrated form:

$$\hat{g} = \int_{-E_c}^{E_c} d\xi_k \hat{G}. \tag{2.4}$$

where $\xi_k = \hbar v_F(k - k_F)$ and E_c defines a cut off energy which is much larger than energies associated with the superconducting state $k_B T_c$. but much smaller than the Fermi energy ϵ_F. The cutoff appears in no physical quantities[27].

2.2 Quasiclassical formalism

The solutions to the Eilenberger equation.

$$i v_F(\hat{\mathbf{k}}) \cdot \vec{\nabla} \hat{g}(i\omega_n, \mathbf{r}, \hat{\mathbf{k}}) + \left[\begin{pmatrix} i\omega_n & -\Delta(\mathbf{r}, \hat{\mathbf{k}}) \\ \Delta^*(\mathbf{r}, \hat{\mathbf{k}}) & -i\omega_n \end{pmatrix} . \hat{g}(i\omega_n, \mathbf{r}, \hat{\mathbf{k}}) \right] = 0. \tag{2.5}$$

$(\hbar = k_B = 1)$ are the quasiclassical Green's functions

$$\hat{g}(i\omega_n, \mathbf{r}, \hat{\mathbf{k}}) = -i\pi \begin{pmatrix} g(i\omega_n, \mathbf{r}, \hat{\mathbf{k}}) & if(i\omega_n, \mathbf{r}, \hat{\mathbf{k}}) \\ -if^\dagger(i\omega_n, \mathbf{r}, \hat{\mathbf{k}}) & -g(i\omega_n, \mathbf{r}, \hat{\mathbf{k}}) \end{pmatrix}. \tag{2.6}$$

where $[A, B] = AB - BA$ denotes a commutator. The Eilenberger equation is supplemented by the normalization condition

$$\hat{g}(i\omega_n, \mathbf{r}, \hat{\mathbf{k}}) \hat{g}(i\omega_n, \mathbf{r}, \hat{\mathbf{k}}) = -\pi^2. \tag{2.7}$$

Here, $\omega_n = (2n+1)\pi T$ is the Matsubara frequency, $\mathbf{r}$ is the center of mass coordinate of the Cooper pair. and the unit vector $\hat{\mathbf{k}}$ is the direction of the relative momentum of the Cooper pair. (In this planar geometry, an isolated vortex line situated at the origin is orientated parallel to the z axis, and both $\mathbf{r}$ and $\hat{\mathbf{k}}$ lie in the x-y plane.)[28] In an applied magentic field, the gap function depends on both $\mathbf{r}$ and $\hat{\mathbf{k}}$.

16

The matrix form of (2.5) is a compact representation of the following three coupled differential equations (omitting the arguments $i\omega_n$, $\mathbf{r}$, and $\hat{\mathbf{k}}$ for brevity, where no confusion can occur):

$$\mathbf{v}_F(\hat{\mathbf{k}}) \cdot \vec{\nabla} g = \Delta^* f - \Delta f^\dagger, \tag{2.8}$$

$$\left(\omega_n - \frac{1}{2}\mathbf{v}_F(\hat{\mathbf{k}}) \cdot \vec{\nabla}\right) f^\dagger = \Delta^* g, \tag{2.9}$$

$$\left(\omega_n + \frac{1}{2}\mathbf{v}_F(\hat{\mathbf{k}}) \cdot \vec{\nabla}\right) f = \Delta g. \tag{2.10}$$

A fourth equation is obtained by the normalization condition (2.7):

$$g = \left(1 - ff^\dagger\right)^{\frac{1}{2}}. \tag{2.11}$$

As suggested by Eilenberger, Eqs. (2.8) - (2.11) resemble transformed transport equations ($\vec{\nabla}$ resembles the convection term, $2\omega_n$ can be interpreted as the transformed $\frac{d}{dt}$). The difference between these and genuine transport equations is the fact that f and $f^\dagger$ cannot be interpreted as probabilities, and a complex $\Delta(\mathbf{r}, \hat{\mathbf{k}})$ makes these functions complex[12].

The appearance of a pole near the real ω-axis in the propagator $g(i\omega_n, \mathbf{r}, \hat{\mathbf{k}})$ defines a *quasiparticle* or long-lived excitation. A local, directional-dependent density of states for quasiparticles of energy E and momentum direction θ is given by:

$$N(\mathbf{r}, \theta, E) = Re\{g(i\omega_n \to E + i\eta, \mathbf{r}, \theta)\}. \tag{2.12}$$

Here, η is a positive infinitesimal quantity, which physically represents an impurity parameter (ie: η shortens the lifetime of quasiparticle).

From $N(\mathbf{r}, \theta, E)$, the local density of states $N(\mathbf{r}, E)$ is obtained by averaging with respect to all θ directions:

$$N(\mathbf{r}, E) = \int_0^{2\pi} \frac{d\theta}{2\pi} N(\mathbf{r}, \theta, E). \tag{2.13}$$

17
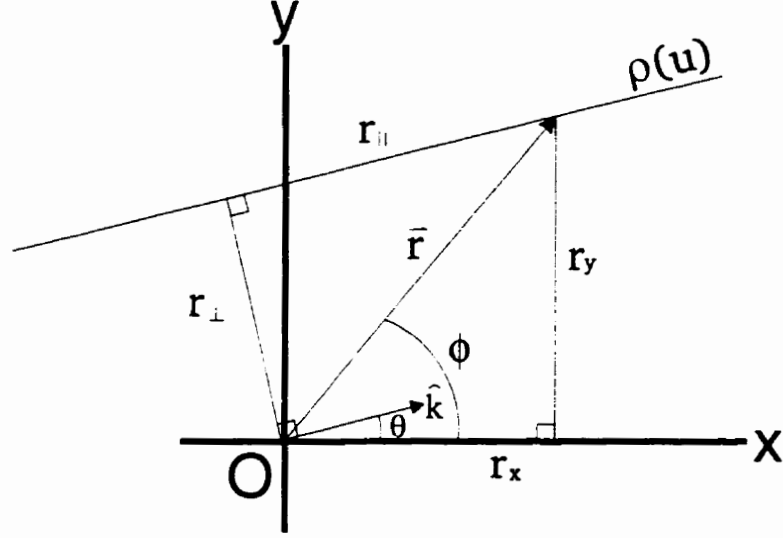
Figure 2.1: The coordinate system for the Riccati transformation method.

2.3 The Riccati transformation method

The Fermi velocity, $\mathbf{v}_F(\hat{\mathbf{k}})$, reflects the anisotropy of the Fermi surface. An isotropic cylindrical Fermi surface is assumed for the work presented here:

$$\mathbf{v}_F(\hat{\mathbf{k}}) = v_F \hat{\mathbf{k}}. \tag{2.14}$$

In a new frame, spanned by the orthogonal unit vectors $\hat{\mathbf{u}} = \cos\theta\hat{\mathbf{x}} + \sin\theta\hat{\mathbf{y}}$ and $\hat{\mathbf{v}} = -\sin\theta\hat{\mathbf{x}} + \cos\theta\hat{\mathbf{y}}$, a fixed point $\mathbf{r} = r_x\hat{\mathbf{x}} + r_y\hat{\mathbf{y}}$ may also be represented by $\mathbf{r} = r_{\|}\hat{\mathbf{u}} + r_{\perp}\hat{\mathbf{v}}$. The unit vector $\hat{\mathbf{k}}$ is denoted by the angle θ measured from the x axis, while ϕ represents the angle from the x axis to the position vector $\mathbf{r}$ (see Figure 2.1).[22]

In this coordinate system, the straight line defined by:

$$\rho(u) = u\hat{\mathbf{u}} + r_{\perp}\hat{\mathbf{v}}, \tag{2.15}$$

is orientated parallel to $\mathbf{k}$ and intersects the point $\mathbf{r}$ at $u = r_{\|}$. Along this line, the

18

directional derivative $\mathbf{v}_F(\hat{\mathbf{k}}) \cdot \vec{\nabla}$ in (2.8) - (2.10) is equivalent to an ordinary derivative:

$$\mathbf{v}_F(\hat{\mathbf{k}}) \cdot \vec{\nabla} = v_F \frac{d}{du}. \tag{2.16}$$

Eq. (2.15) is known as the *quasiparticle path* and $r_\perp$ has the natural meaning of an *impact parameter*.

Therefore, the Eilenberger equations along the quasiparticle path are given as:

$$\partial_{\parallel} g(i\omega_n, \rho(u), \theta) = \bar{\Delta}^*(\rho(u), \theta)\bar{f}(i\omega_n, \rho(u), \theta) - \bar{\Delta}(\rho(u), \theta)\bar{f}^\dagger(i\omega_n, \rho(u), \theta). \tag{2.17}$$

$$\left\{\omega_n - \frac{1}{2}(\partial_{\parallel} - i\partial_{\parallel}\varphi)\right\}\bar{f}^\dagger(i\omega_n, \rho(u), \theta) = \bar{\Delta}^*(\rho(u), \theta)g(i\omega_n, \rho(u), \theta), \tag{2.18}$$

$$\left\{\omega_n + \frac{1}{2}(\partial_{\parallel} + i\partial_{\parallel}\varphi)\right\}\bar{f}(i\omega_n, \rho(u), \theta) = \bar{\Delta}(\rho(u), \theta)g(i\omega_n, \rho(u), \theta). \tag{2.19}$$

where $\partial_{\parallel} = \frac{d}{du}$, $\partial_{\parallel}\varphi = -\frac{r_\perp}{r^2}$, and $r = \sqrt{u^2 + r_\perp^2}$. The phase $e^{i\varphi} = (r_x + ir_y)/r$ has been factored out of the anomalous Green's functions and pair potential for convenience (ie: $f = \bar{f}e^{i\varphi}$, $f^\dagger = \bar{f}^\dagger e^{-i\varphi}$, $\Delta = \bar{\Delta}e^{i\varphi}$, and $\Delta^* = \bar{\Delta}^* e^{-i\varphi}$). All energies and lengths are measured in units of the uniform gap Δ_0 at $T = 0$ and the coherence length $\xi_0 = v_F/\Delta_0$, respectively[28].

The Riccati transformation method uses the parameterization devised by Schopohl and Maki[22]:

$$\bar{f} = \frac{2\bar{a}}{1 + \bar{a}\bar{b}}, \quad \bar{f}^\dagger = \frac{2\bar{b}}{1 + \bar{a}\bar{b}}, \quad g = \frac{1 - \bar{a}\bar{b}}{1 + \bar{a}\bar{b}}. \tag{2.20}$$

This transformation decouples the Eilenberger equations and enormously simplifies the numerical computation.

Substituting (2.20) into (2.17) - (2.19) results in the Riccati equations (for a given ω_n, $r_\perp$, and θ):

$$\frac{d}{du}\bar{a}(u) = \bar{\Delta}(u) - \left\{2\omega_n - i\frac{r_\perp}{r^2} + \bar{\Delta}^*(u)\bar{a}(u)\right\}\bar{a}(u), \tag{2.21}$$

$$\frac{d}{du}\bar{b}(u) = -\bar{\Delta}^*(u) + \left\{2\omega_n - i\frac{r_\perp}{r^2} + \bar{\Delta}(u)\bar{b}(u)\right\}\bar{b}(u). \tag{2.22}$$

19

For $i\omega_n$ situated in the upper half of the complex plane, the physical solution for $\bar{a}(r_{\parallel})$ is found by integrating (2.21) as an initial value problem from $u = -\infty$ to $u = r_{\parallel}$ with increasing u-values. On the other hand, the physical solution for $\bar{b}(r_{\parallel})$ is found by integrating (2.22) as an initial value problem from $u = \infty$ to $u = r_{\parallel}$ with decreasing u-values[29].

Initial values for (2.21) and (2.22) are obtained by looking at solutions far from the isolated vortex:

$$\bar{a}_{-\infty} = \frac{\sqrt{\omega_n^2 + |\bar{\Delta}(\rho(-\infty),\theta)|^2} - \omega_n}{\bar{\Delta}^*(\rho(-\infty),\theta)}.$$

$$\bar{b}_{+\infty} = \frac{\sqrt{\omega_n^2 + |\bar{\Delta}(\rho(+\infty),\theta)|^2} - \omega_n}{\bar{\Delta}(\rho(+\infty),\theta)}. \tag{2.23}$$

The gap function for an isolated vortex is expressed as a decomposition of its spatial and momentum components:

$$\bar{\Delta}(\mathbf{r},\theta) = \bar{\Delta}(\mathbf{r})\bar{\Delta}(\theta). \tag{2.24}$$

At the core center, the spatial component is zero. It increases to a finite, temperature-dependent value as one moves into the bulk region. This behaviour is modeled by[22, 23, 24]:

$$\bar{\Delta}(\mathbf{r}) = \bar{\Delta}(T)\tanh(r) \tag{2.25}$$

where $\bar{\Delta}(T)$ is the uniform temperature-dependent gap given by BCS theory. Here, we set $\bar{\Delta}(T) = 1$.

The k-space variation of the gap function $\bar{\Delta}(\theta)$ determines the nature of the pairing. Table 2.1 defines the seven different gaps investigated in this thesis, several of which are considered as possibilities in high-T_c superconductors.

To obtain the local density of states (2.13), the Green's function $g(i\omega_n \to E + i\eta, \mathbf{r}, \theta)$ is calculated using the Riccati transformation method with $\omega_n = \eta - iE$. The

Order Parameter	$\Delta(\theta)$
s	1.0
$d_{x^2-y^2}$	$\cos(2\theta)$
sixfold anisotropic s	$1 + 0.5\cos(6\theta)$
$d_{x^2-y^2} + i\alpha d_{xy}$	$\cos(2\theta) + 0.2i\sin(2\theta)$
$d_{x^2-y^2} + \alpha s$	$\cos(2\theta) + 0.2$
$s + \alpha d_{x^2-y^2}$	$1 + 0.2\cos(2\theta)$
g	$\cos(4\theta)$

Table 2.1: Order parameter definitions with $\alpha = 0.2$.

differential equations (2.21) and (2.22) are numerically integrated using an adaptive stepsize fourth-order Runge-Kutta scheme. The integration in (2.13) is performed using Simpson's rule of integration. which is also good to fourth-order.

Chapter 3

Results and Discussions

This chapter presents a study of the local density of states $\mathcal{N}(\mathbf{r}, E)$ using the method described in Section 2.3. As a reminder, all quantities are dimensionless: the energies. lengths. and density of states are quoted in units of Δ_0 (the uniform gap at zero temperature). ξ_0 (the coherence length). and $\mathcal{N}_0$ (the normal metal density of states at the Fermi energy). respectively.

3.1 Local density of states in the bulk

Before focusing attention on the vortex core. it is perhaps beneficial to first consider the superconducting bulk. In this region ($\mathbf{r} \to \infty$). the directional-dependent density of states is given by:

$$\mathcal{N}(\theta, E) = Re \left\{ \frac{|E|}{\sqrt{E^2 - |\Delta(\theta)|^2}} \right\} \tag{3.1}$$

which is nonzero only when $E > |\Delta(\theta)|$. In Figure 3.1. the local density of states vs energy E is calculated for a point far from the vortex center. Shown are the s-wave. d-wave. $d + i\alpha d$-wave. and sixfold anisotropic s-wave gaps.

For an s-wave superconductor. there are no states for energies less than $|\Delta|$. The
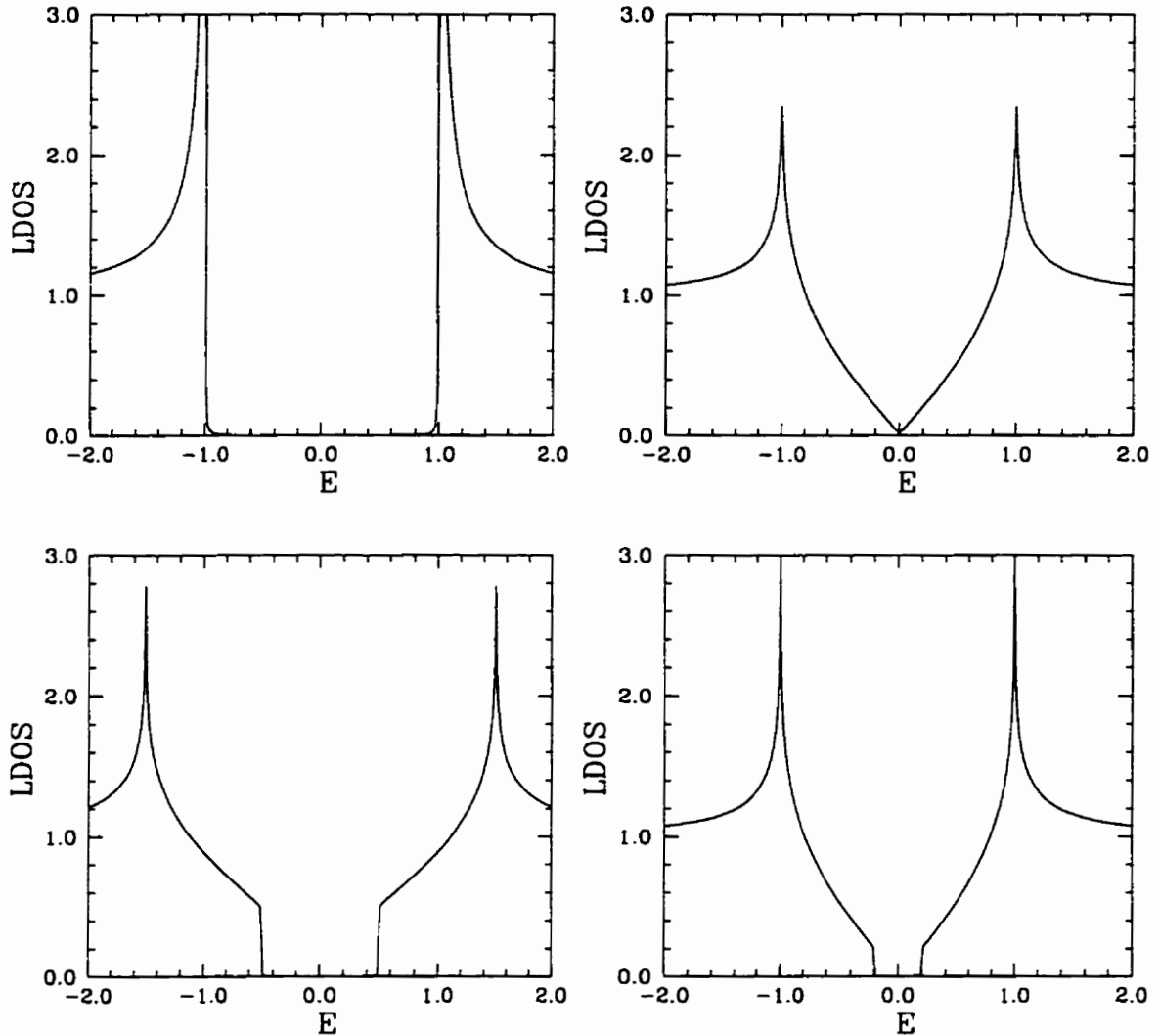
Figure 3.1: Local density of states $\mathcal{N}(E, \mathbf{r})$ vs energy E far from the vortex center ($\eta = 0.001$). The results are calculated for the point $r = 10$ along the x-axis, but represents the bulk LDOS in general. Shown are the s-wave gap (upper left), $d_{x^2-y^2}$-wave gap (upper right), $d_{x^2-y^2} + 0.2id_{xy}$-wave gap (lower right) and an anisotropic s-wave gap, $\Delta(\theta) = 1 + 0.5\cos(6\theta)$, (lower left).

addition of anisotropy to the s-wave causes a broadening of the peak edge. As seen in the anisotropic s-wave gap, the broadening extends over a range $E = 1 - \alpha$ to $1 + \alpha$ (here, $\alpha = 0.5$). In contrast, a pure d-wave order parameter vanishes along certain θ directions, thereby allowing states to exist for all values of E. The behaviour of the $d + i\alpha d$-wave order parameter (with $\alpha = 0.2$) is similar to the d-wave since the d_{xy} component is small. However, the order parameter is fully gapped, and for $|E| < \alpha$, there are no states.

In the vicinity of a vortex, single-particle states exist and Eq. (3.1) no longer holds. In the following calculations, only the positive energy values are discussed, since the local density of states is a symmetric function of E.

3.2   Comparison between s-wave and $d_{x^2-y^2}$-wave

The local density of states around a vortex core is considered for the s-wave:

$$\Delta(\theta) = 1, \tag{3.2}$$

and $d_{x^2-y^2}$-wave:

$$\Delta(\theta) = \cos(2\theta), \tag{3.3}$$

order parameters. Our calculations (shown in Figure 3.2) are in good agreement with those of Schopohl and Maki[22].

Figure 3.2 illustrates the spatial dependency of the LDOS for energies $E = 0$, $E = 0.2$, and $E = 0.6$. The quasiparticle excitation is circular for the s-wave case, and has a fourfold symmetry in a d-wave superconductor. At $E = 0$, both feature a large, zero-bias peak at the vortex center. The d-wave also has small peak ridges extending along the line $y = \pm x$.
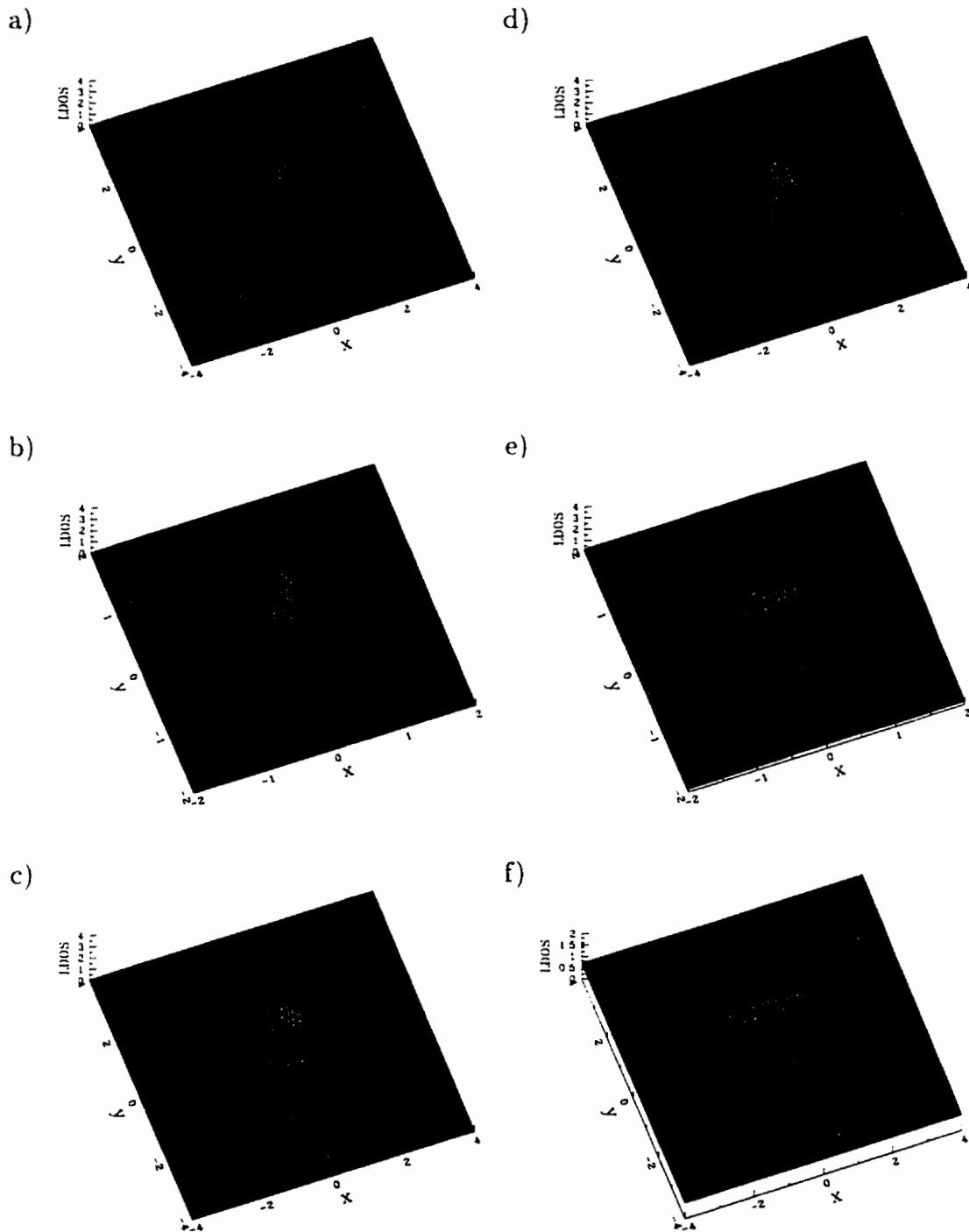
Figure 3.2: Comparison of the local density of states $N(E, \mathbf{r})$ vs $\mathbf{r}$ between the s-wave and $d_{x^2-y^2}$-wave. Results for s-wave are shown for energies a) $E = 0.0$, b) $E = 0.20$, and c) $E = 0.60$. Results for $d_{x^2-y^2}$-wave are shown for energies d) $E = 0.0$, e) $E = 0.20$, and f) $E = 0.60$. The height of the zero-bias peak at the vortex center has been truncated in (a) and (d).
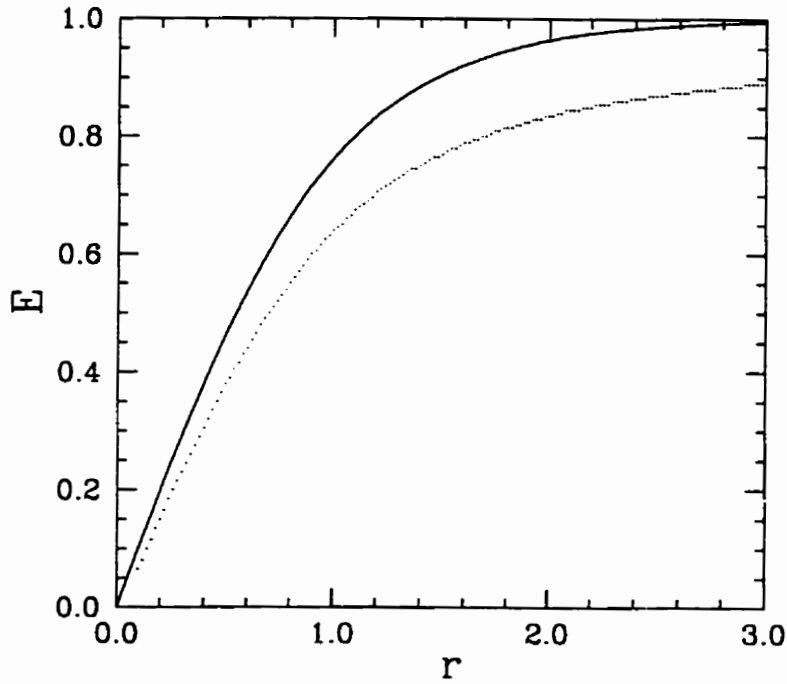
Figure 3.3: Plot of the peak energy vs distance r from the vortex center for an s-wave superconductor (dotted line). Also shown is the function $E = \tanh(r)$ (solid line).

For the s-wave case. as E increases. the zero-bias peak splits (into a positive and negative bias peak). and the peak is found further from the center. Due to the isotropic nature of the s-wave pairing. a circular distribution is seen in Figures 3.2(b) and (c). Figure 3.3 shows how the zero-bias peak *evolves* with increasing energy. This plot represents the energy and corresponding radius of the peak in the LDOS. For comparison, the relationship:

$$E = \tanh(r) \tag{3.4}$$

is plotted as well. As a rough approximation, the excitations occur when $E \sim |\Delta(\mathbf{r})|$.

Figure 3.4 shows the LDOS for an s-wave superconductor as a function of energy at three different radial distances from the vortex center. The shape of the peak is not symmetric about its maxima, but rather smears out towards lower energies, while decaying rapidly for higher ones.

26
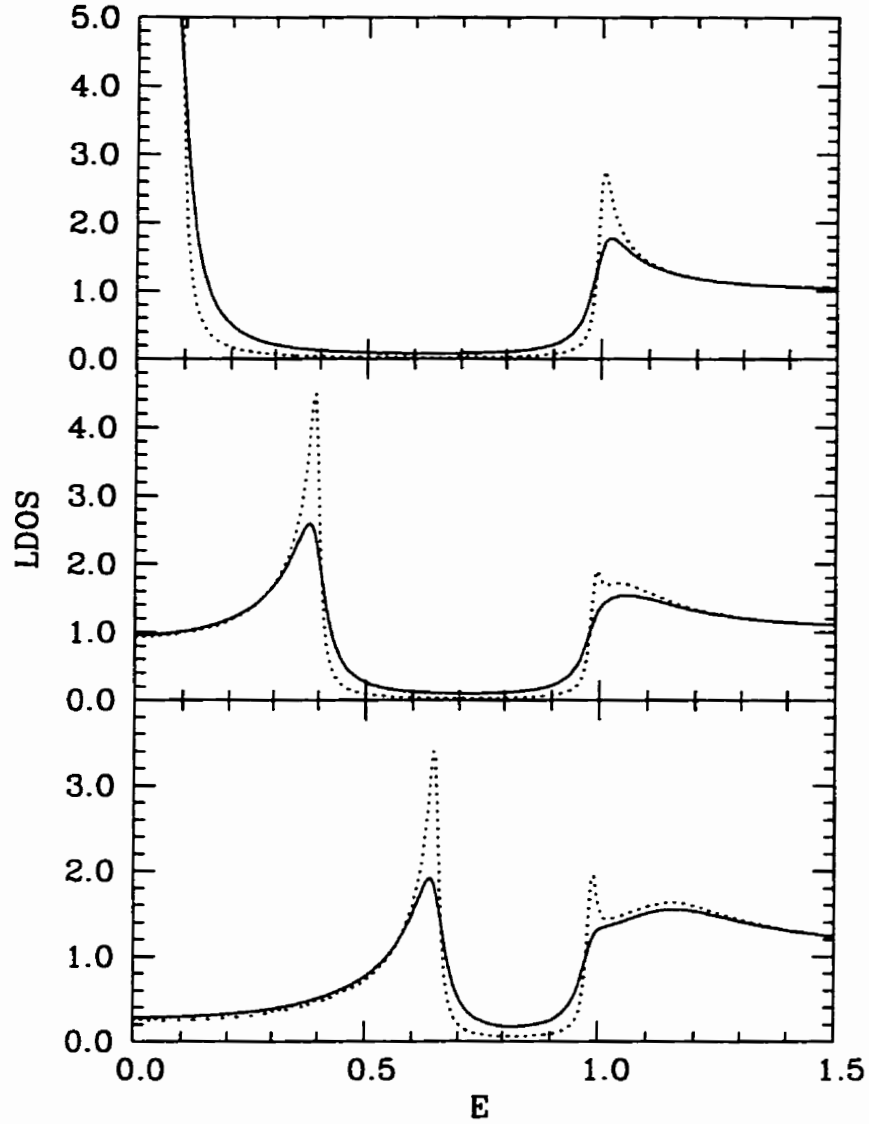
Figure 3.4: Local density of states $\mathcal{N}(E, \mathbf{r})$ vs energy E for an s-wave superconductor. The position $\mathbf{r}$ is held fixed with magnitude of $r = 0.1$ (upper), $r = 0.5$ (middle), and $r = 1.0$ (lower). The value of the smearing parameter is $\eta = 0.03$ (solid line) and $\eta = 0.01$ (dashed line).
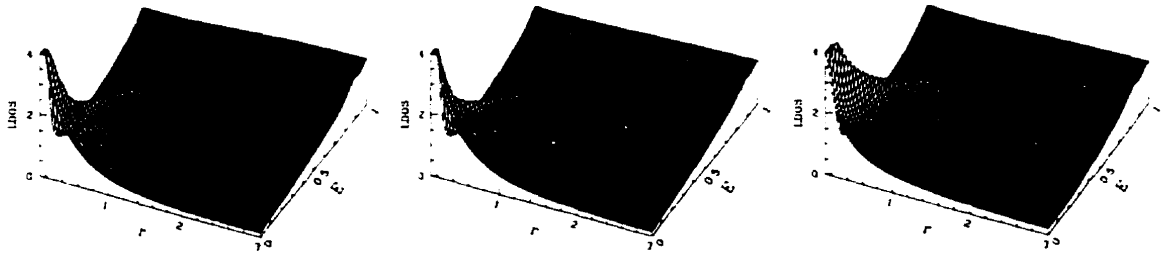
Figure 3.5: Local density of states $N(E, r)$ as a function of energy E and distance r from the vortex center, along the direction $o = 0°$ (left), $o = 15°$ (middle), and $o = 45°$ (right) for a pure $d_{x^2-y^2}$-wave order parameter. The height has been truncated in all figures.

Also shown in Figure 3.4 are the effects of the impurity parameter η. Lower values correspond to fewer lifetime effects resulting from impurity scattering, etc.

In contrast to the s-wave, the d-wave has a fourfold symmetric local density of states. As shown in Figures 3.2(d) and (e), the quasiparticles form a distribution which curve around the vortex core, forming a 'square'-like structure at the center. In the limit $E \rightarrow 0$, the distribution rotate $45°$ and the curvature closes in on the core. As shown in Figure 3.2(c), there are peaks that still exist along the lines $y = \pm x$.

Figure 3.5 shows the evolution of the zero-bias peak, which splits into various peaks depending on the radial direction. Figure 3.6 shows the LDOS at nine different points (three points with the same magnitude of r as those in Figure 3.4, taken along three separate directional lines extending from the center).

The same results for the $d_{x^2-y^2}$-wave order parameter are found when the form $|\cos(2\theta)|$ is used instead of $\cos(2\theta)$. This corresponds to the case where the sign of the pair potential Eq. (2.24) does not change. As might be expected, the LDOS is sensitive only to the magnitude of the order parameter.
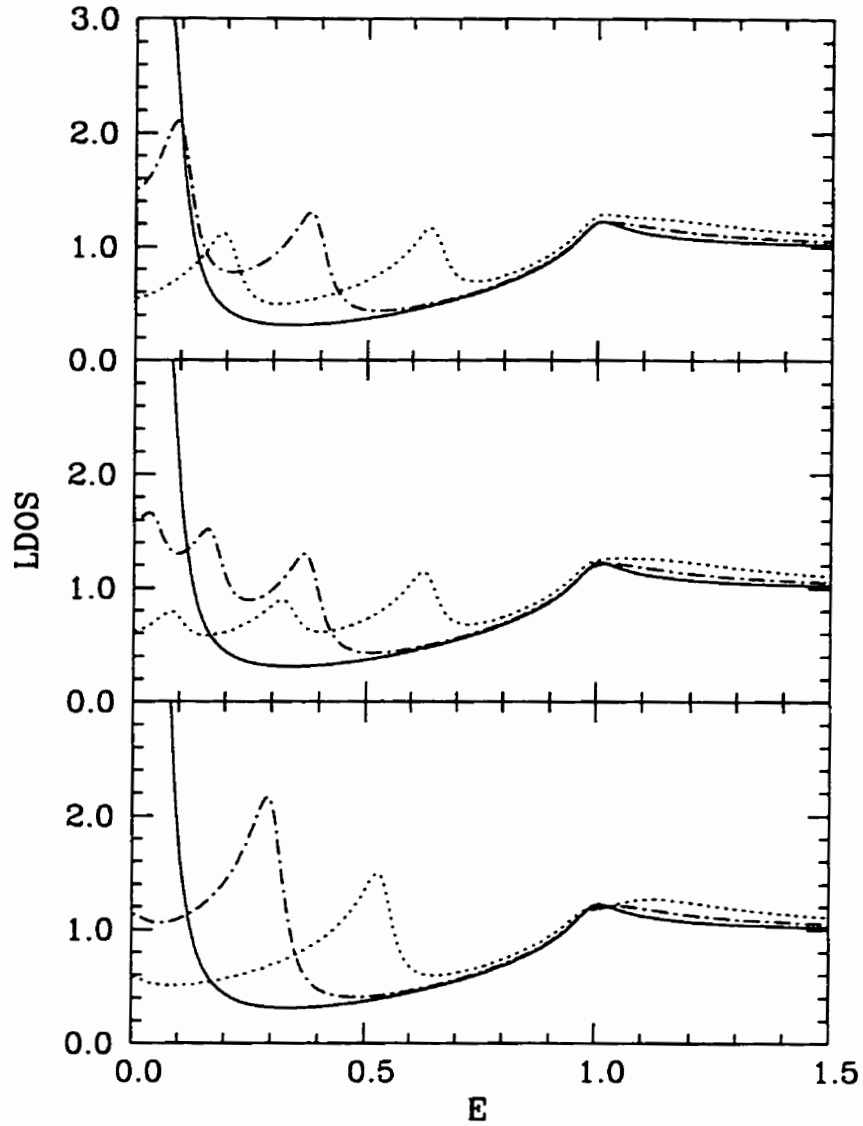
Figure 3.6: Local density of states $N(E, \mathbf{r})$ vs energy E for $d_{x^2-y^2}$-wave superconductivity ($\eta = 0.03$). The position $\mathbf{r}$ is held fixed with magnitude of $r = 0.1$ (solid line), $r = 0.5$ (dash-dot line), and $r = 1.0$ (dotted line). The angle of $\mathbf{r}$ from the x-axis corresponds to $\phi = 0°$ (upper figure), $\phi = 15°$ (middle figure), and $\phi = 45°$ (lower figure).

29

3.3 Sixfold anisotropic s-wave

In this section. the properties of a sixfold anisotropic s-wave gap:

$$\Delta(\theta) = 1 + \alpha \cos(6\theta). \tag{3.5}$$

with $\alpha = 0.5$ are presented. An order parameter of this form was first proposed by Hayashi $et\ al.$[24] to help explain the features found in STM experiments on the compound NbSe$_2$. However. instead of Eq. (2.25). Hayashi calculated a self-consistent solution to $\Delta(\mathbf{r})$. Nevertheless. the results found here are in good agreement with their work. This indicates that the structure of the local density of states originates from the k-space variations of the order parameter $\Delta(\theta)$.

Figure 3.7(a) reveals a sixfold symmetry in the spatial structure of the local density of states. The plot is for $E = 0.2$ with an impurity parameter of $\eta = 0.03$. To help clarify the behaviour. an outline of the quasiparticle paths is shown in 3.7(b).

The evolution of the quasiparticle excitations along different radial lines is shown in Figures 3.7(c).(d). and (e). The zero-bias peak splits into several peak ridges in each plot. Along all directions. the common characteristic is the formation of a lower peak at $E \approx 0.5$ and an upper peak at $E \approx 1.5$ as the radial distance increases. These directionally-independent peaks are a result of the anisotropy of the s-wave gap. which is distributed from $E = 1 - \alpha$ to $E = 1 + \alpha$. As well. the LDOS as a function of energy is shown in Figures 3.7(f) and (g) for three separate spatial points.

In Figure 3.8. the LDOS as a function of $\mathbf{r}$ is shown for three increasing energy values $E = 0$. $E = 0.15$, and $E = 0.32$. The calculations correspond to an impurity parameter of $\eta = 0.03$. however the scale is one that focuses attention on the underlying structure instead of the peaks (ie: values for $N(E, \mathbf{r}) > 0.5$ are not differentiated in the plot). At $E = 0$. a sixfold star centered at the core with the rays oriented

30
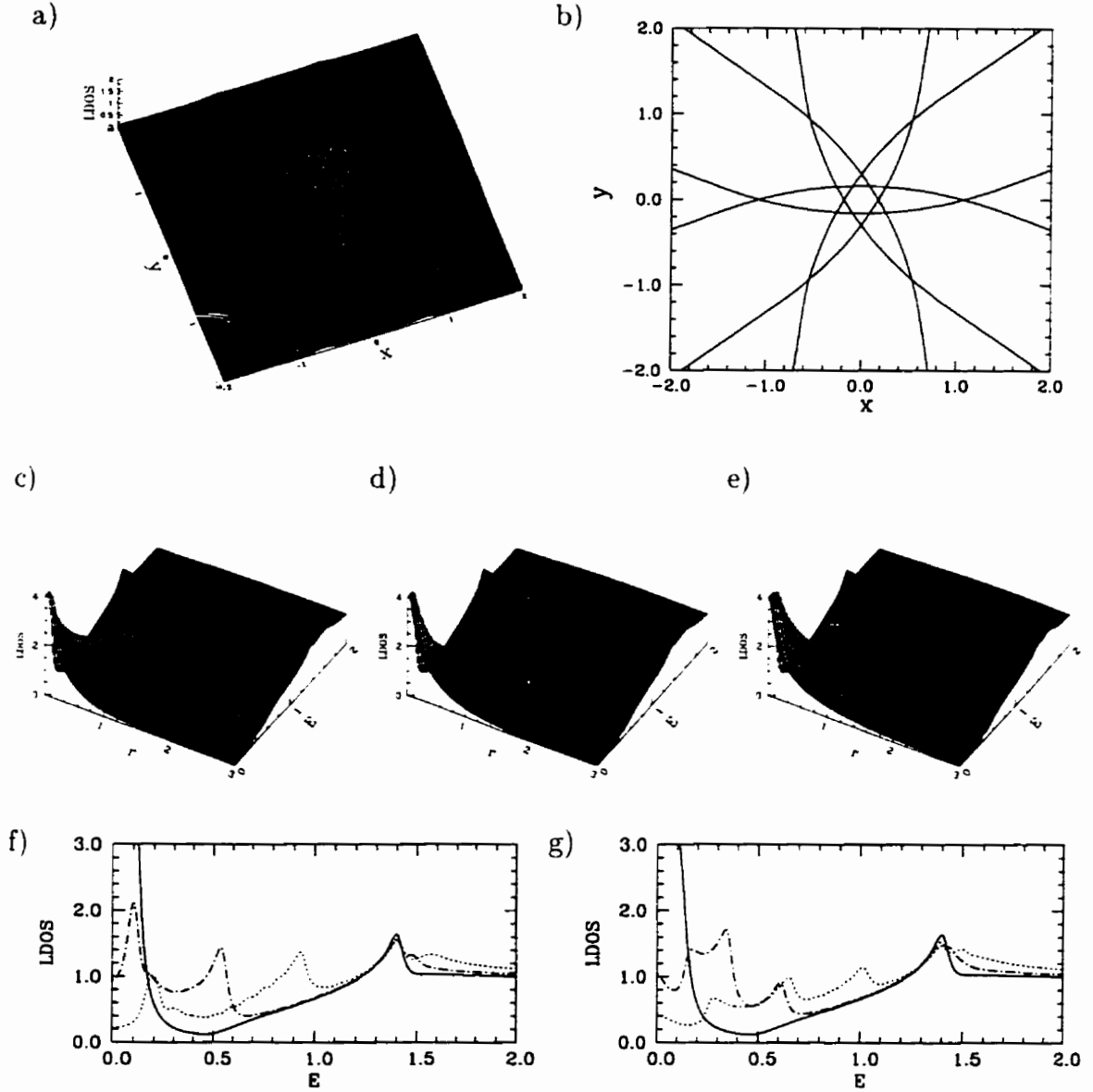
Figure 3.7: Results for a sixfold anisotropic s-wave order parameter $\Delta(\theta) = 1 + 0.5\cos(6\theta)$. The spatial dependence at $E = 0.2$ is shown in (a). The corresponding peaks are outlined in (b). The evolution of the quasiparticle excitations along a radial line is shown for radial angles c) $\phi = 0°$, (d) $\phi = 15°$, and (e) $\phi = 30°$. The height of the zero-bias peak has been truncated. Cross sections of the evolution showing the LDOS as a function of energy are shown for (f) $\phi = 0°$ and (g) $\phi = 30°$. In (f) and (g), three radial distances are shown, $r = 0.1$ (solid line), $r = 0.5$ (dot-dash line) and $r = 1.0$ (dotted line).

31
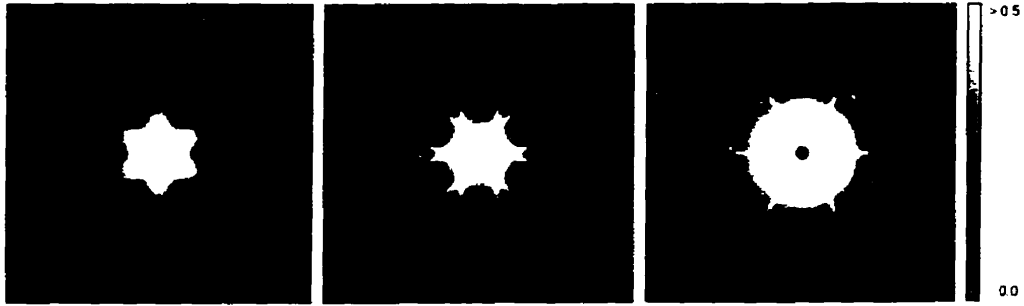
Figure 3.8: Local density of states for an anisotropic s-wave superconductor. $\Delta(\theta) = 1 + 0.5\cos(6\theta)$. The images are calculated for energies $E = 0.0$ (left), $E = 0.15$ (middle), and $E = 0.32$ (right) on a grid of size $4\xi_0 \times 4\xi_0$.

away from the x axis is seen. At an intermediate energy $E = 0.15$, each ray has split into two parallel rays. As the energy is increased to $E = 0.32$, the star becomes more extended and the heads of each ray spreads out. The orientation of the star has rotated by $30°$. These results are similar to the description of STM experiments on NbSe$_2$ [16, 17, 18]. In this way, the anisotropic s-wave gap well reproduces the experimental features mentioned in Section 1.4.

Strictly speaking, no effort was made to fit material parameters appropriate to NbSe$_2$ into these calculations. These results apply to a model superconductor with an order parameter given by Eq. (3.5).

3.4 $d_{x^2-y^2} + i\alpha d_{xy}$-wave and g-wave

The symmetry of the order parameter can now be observed directly with STM experiments. In light of this, we calculate the local density of states for a $d_{x^2-y^2} + i\alpha d_{xy}$-wave superconductor:

$$\Delta(\theta) = \cos(2\theta) + i\alpha\sin(2\theta), \tag{3.6}$$

32

and a g-wave superconductor:

$$\Delta(\theta) = \cos(4\theta). \tag{3.7}$$

Recently, the $d + id$ gap has been invoked to explain the thermal conductivity data on $Bi_2Sr_2CaCu_2O_8$ in finite magnetic fields[30]. Figure 3.9 shows the results for the $d + i\alpha d$-wave gap with $\alpha = 0.2$. A fourfold pattern similar to the pure d-wave is seen, however the peaks are slightly skewed.

Another unconventional order parameter is the g-wave, which has eightfold symmetry. The g-wave recovers information in band model theories involving hopping to nearest neighbours[31]. Figure 3.10 shows the resulting local density of states for such a gap.

3.5 Mixing order parameters

Finally, we investigate order parameters that are admixtures of the conventional s-wave and d-wave. In particular, a $s + \alpha d$-wave gap:

$$\Delta(\theta) = 1 + \alpha \cos(2\theta), \tag{3.8}$$

and a $d + \alpha s$-wave:

$$\Delta(\theta) = \cos(2\theta) + \alpha, \tag{3.9}$$

are presented. In these calculations, $\alpha = 0.2$ is used.

Figure 3.11 shows the results for the $s + \alpha d$-wave gap, an order parameter that is mostly s-wave, with a small mixing of d-wave. The resulting distribution of the LDOS is an elongated circle, with major axis in the x-direction. This order parameter is fully gapped, and in the evolution plots, there are directionally-independent ridges forming for $E = 1 - \alpha$ and $E = 1 + \alpha$.

Figure 3.12 shows the results for the $d + \alpha s$ order parameter. Here, a twofold symmetry is seen. but the overall pattern is closely related to the fourfold structure of the d-wave. The peaks which flow in the y direction do not approach the core as tightly as those in the x direction. The resulting shape in the center is a square that is elongated in the x-direction.
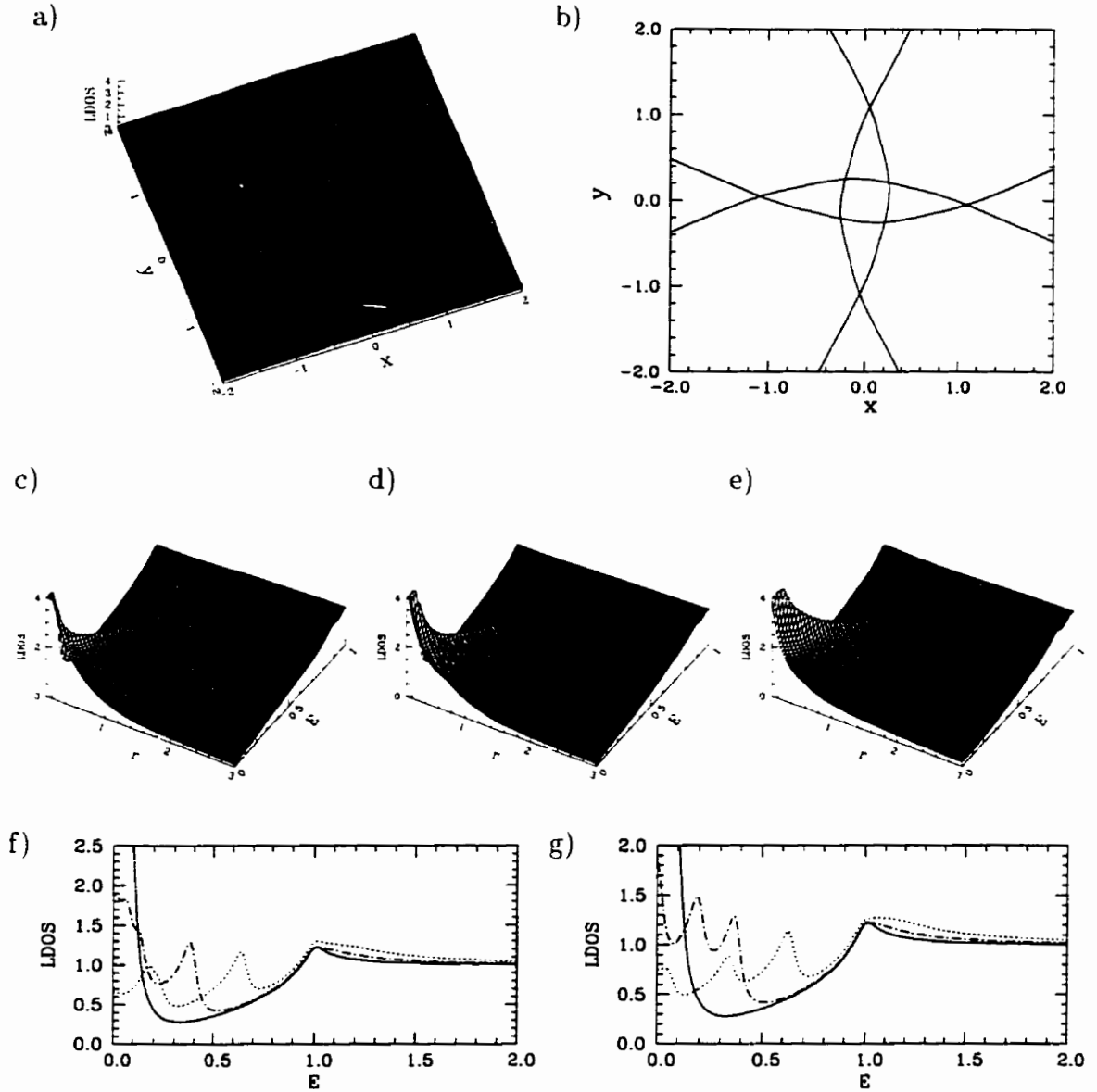
Figure 3.9: Results for the $d_{x^2-y^2} + \alpha i d_{xy}$-wave order parameter $\Delta(\theta) = \cos(2\theta) + 0.2i\sin(2\theta)$. The spatial dependence at $E = 0.2$ is shown in (a). The corresponding peaks are outlined in (b). The evolution of the quasiparticle excitations along a radial line is shown for radial angles c) $\phi = 0°$, (d) $\phi = 15°$, and (e) $\varphi = 45°$. The height of the zero-bias peak has been truncated. Cross sections of the evolution showing the LDOS as a function of energy are shown for (f) $\phi = 0°$ and (g) $\phi = 15°$. In (f) and (g), three radial distances are shown, $r = 0.1$ (solid line), $r = 0.5$ (dot-dash line) and $r = 1.0$ (dotted line).
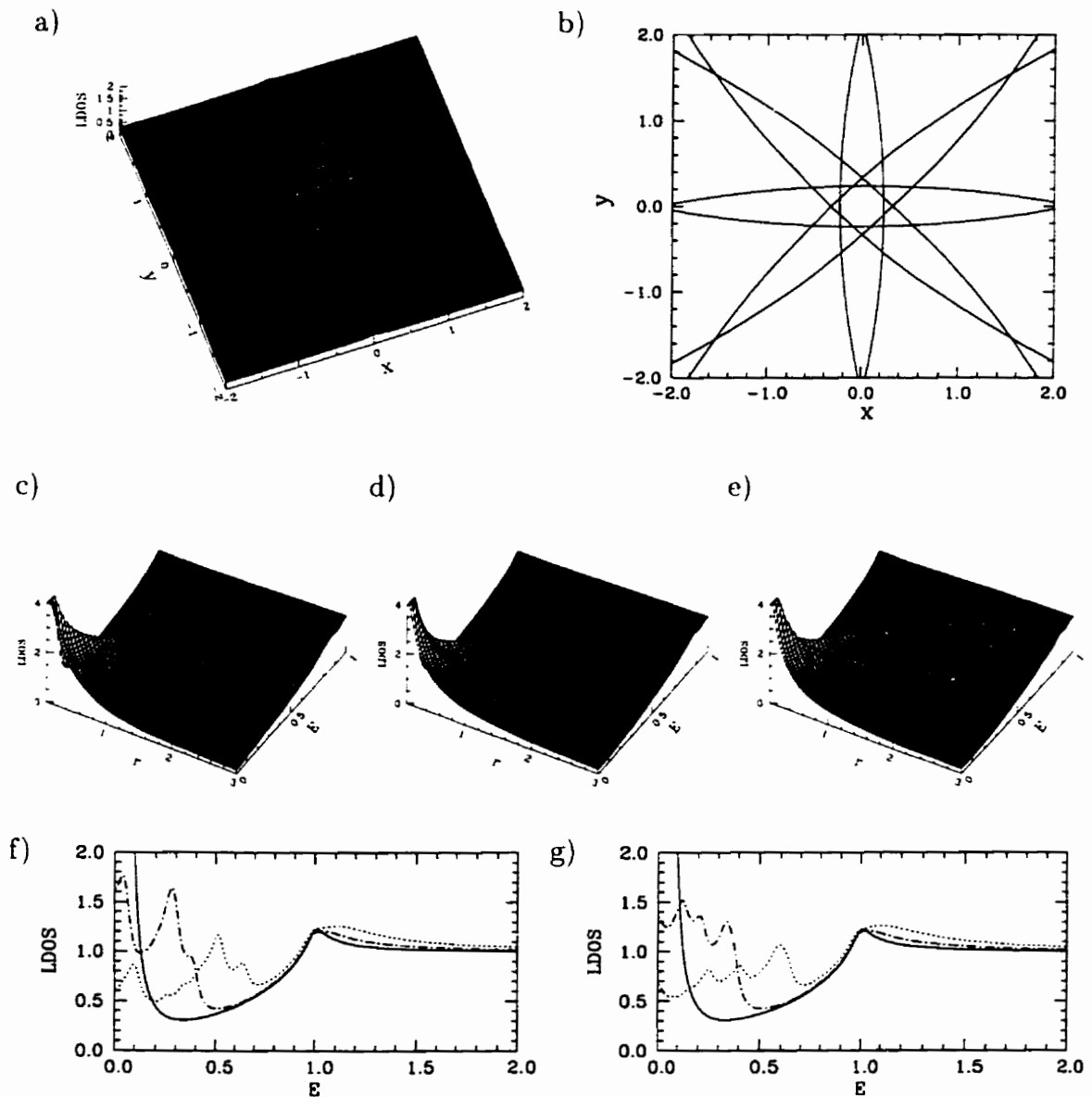
Figure 3.10: Results for the g-wave order parameter $\Delta(\theta) = \cos(4\theta)$. The spatial dependence at $E = 0.2$ is shown in (a). The corresponding peaks are outlined in (b). The evolution of the quasiparticle excitations along a radial line is shown for radial angles c) $\phi = 0°$, (d) $\phi = 15°$, and (e) $\phi = 22.5°$. The height of the zero-bias peak has been truncated. Cross sections of the evolution showing the LDOS as a function of energy are shown for (f) $\phi = 0°$ and (g) $\phi = 15°$. In (f) and (g), three radial distances are shown, $r = 0.1$ (solid line), $r = 0.5$ (dot-dash line) and $r = 1.0$ (dotted line).
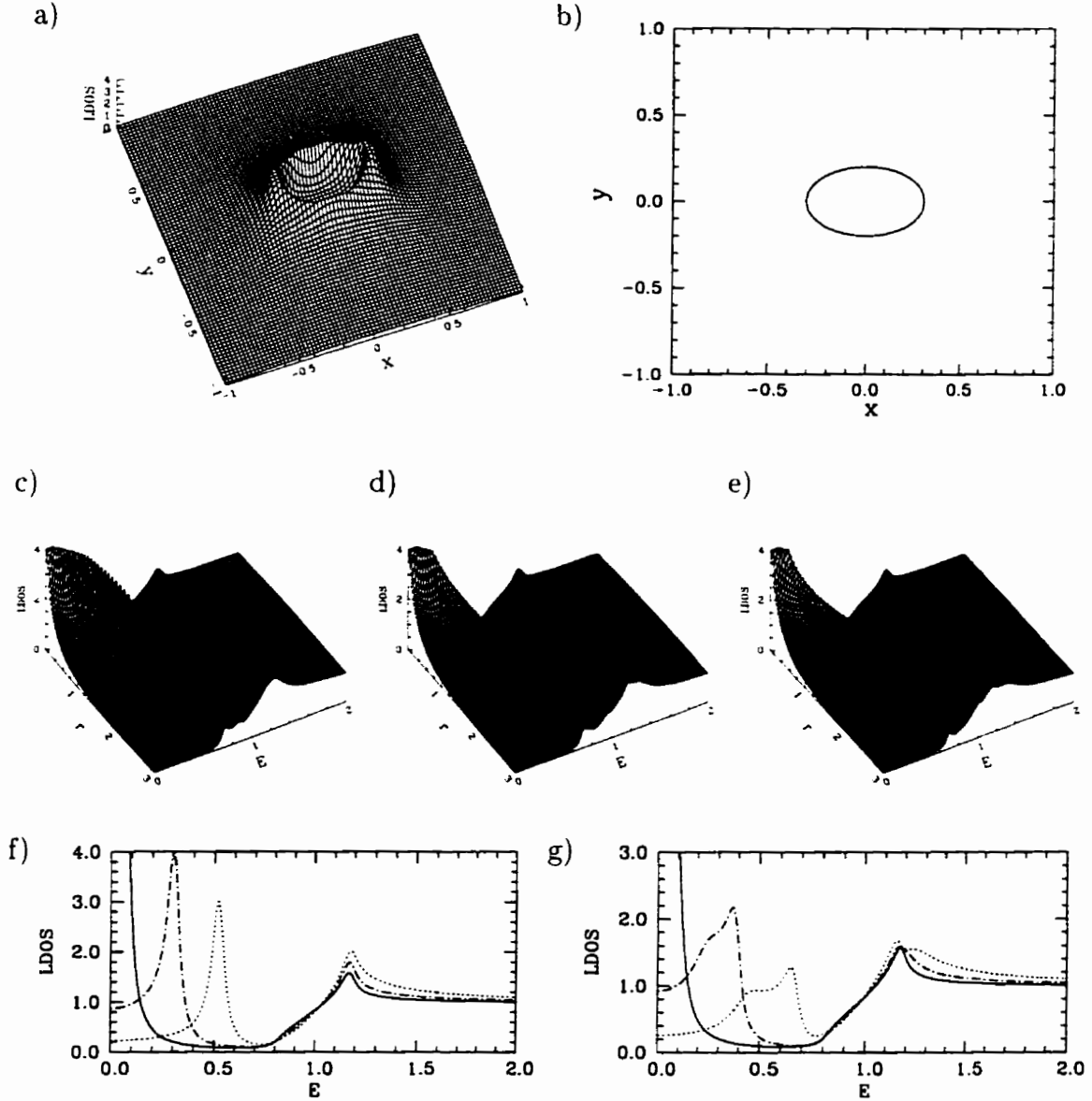
Figure 3.11: Results for the $s + \alpha d_{x^2-y^2}$-wave order parameter $\Delta(\theta) = 1 + 0.2\cos(2\theta)$. The spatial dependence at $E = 0.2$ is shown in (a). The corresponding peaks are outlined in (b). The evolution of the quasiparticle excitations along a radial line is shown for radial angles c) $\phi = 0°$, (d) $\phi = 15°$, and (e) $\phi = 30°$. The height of the zero-bias peak has been truncated. Cross sections of the evolution showing the LDOS as a function of energy are shown for (f) $\phi = 0°$ and (g) $\phi = 30°$. In (f) and (g), three radial distances are shown, $r = 0.1$ (solid line), $r = 0.5$ (dot-dash line) and $r = 1.0$ (dotted line).

37

a)

b)

c)

d)

e)

f)

g)
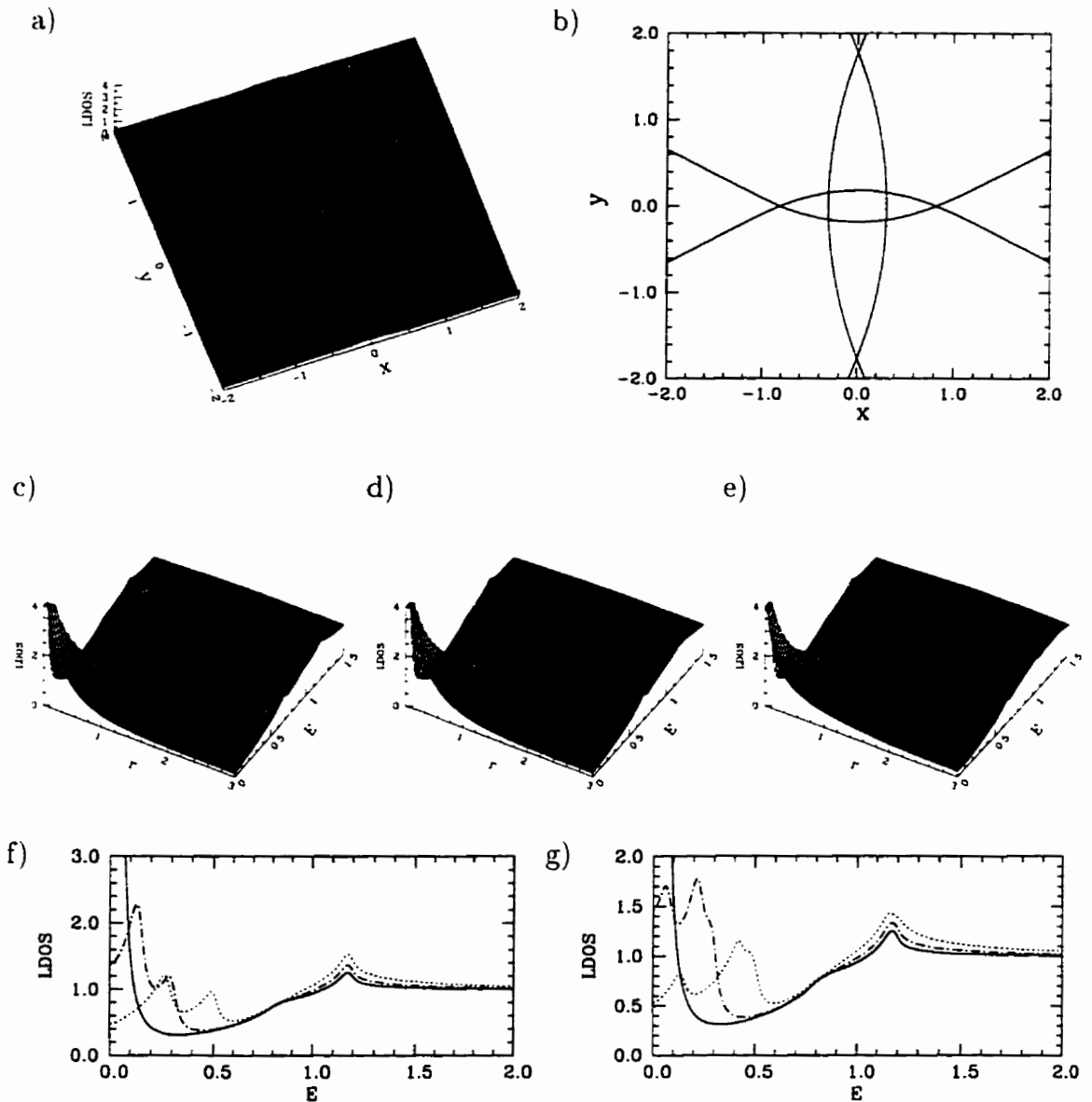
Figure 3.12: Results for the $d_{x^2-y^2} + \alpha s$-wave order parameter $\Delta(\theta) = \cos(2\theta) + 0.2$. The spatial dependence at $E = 0.2$ is shown in (a). The corresponding peaks are outlined in (b). The evolution of the quasiparticle excitations along a radial line is shown for radial angles c) $\phi = 0°$, (d) $\phi = 15°$, and (e) $\phi = 45°$. The height of the zero-bias peak has been truncated. Cross sections of the evolution showing the LDOS as a function of energy are shown for (f) $\phi = 0°$ and (g) $\phi = 15°$. In (f) and (g), three radial distances are shown, $r = 0.1$ (solid line), $r = 0.5$ (dot-dash line) and $r = 1.0$ (dotted line).

38

Chapter 4

Conclusion

4.1 Summary

Here a final review is given of what was done in the preceding chapters. In this work.
the local density of states around an isolated vortex is calculated by solving the qua-
siclassical Eilenberger equations. The approach outlined in this thesis is appropriate
for clean superconductors. in which a quasiparticle passing near a vortex travels along
a straight line parallel to the direction of its momentum. In this framework. we make
use of a parameterization that transforms the Eilenberger equations into ordinary
differential equations.

In Chapter 3, we presented the results of our numerical study. We find that the
LDOS is influenced by the k-space variations of the order parameter. and for several
different order parameters. we catalog these effects.

4.2 Concluding remarks

Results of the calculations in the local density of states for an anisotropic order parameter agree quite well with the experimental results on $NbSe_2$. However, in superconductors such as the high-T_c copper oxides, the coherence length is short, and the quasiclassical approach may not be appropriate. While it is likely that further corrections are required to explain experimental results for these cuprates, we believe that the calculations performed here remain at least qualitatively correct.

Finally, aside from calculating the local density of states, the method presented here may be used to study other physical observables. For instance, the current around a vortex, or a self-consistent pair potential, are directly calculated from the quasiclassical Green's functions.

Bibliography

[1] Excellent overall references include: R.D. Parks. ed.. *Superconductivity. vol. 1.* Marcel Dekker Inc.. New York. 1989. C.P. Poole Jr.. H.A. Farach. and R.J. Creswick. *Superconductivity.* Academic Press. Inc.. Toronto. 1995.

[2] References on the theory of superconductivity: P. DeGennes. *Superconductivity of Metals and Alloys.* W.A. Benjamin Inc.. New York. 1966. J.R. Schrieffer. *Theory of Superconductivity.* W.A. Benjamin Inc.. New York. 1964. G. Rickayzen. *Theory of Superconductivity.* John Wiley & Sons. New York. 1965.

[3] High-T_c references: J.C. Phillips. *Physics of High-T_c Superconductors.* Academic Press. Inc.. Toronto. 1989. N.M. Plakida. *High-Temperature Superconductivity: Experiment and Theory.* Springer-Verlag. New York. 1995.

[4] H.K. Onnes. Leiden Comm. **119b** (1911).

[5] W. Meissner and R. Ochsenfeld. Naturwiss. **21,** 787 (1933).

[6] F. London and H. London. Proc. Roy. Soc. Lond. **A149,** 71 (1935).

[7] A.B. Pippard. Proc. Roy. Soc. Lond. **A216,** 547 (1953).

[8] V.L. Ginzburg and L.D. Landau. JETP (USSR) **20,** 1064 (1950).

[9] A.A. Abrikosov. JETP (USSR) **32**, 1442 (1957). Translated in: Soviet Phys. JETP **5**, 1174 (1957).

[10] J. Bardeen. L.N. Cooper. and J.R. Schrieffer. Phys. Rev. **108**, 1175 (1957).

[11] L.P. Gor'kov. JETP (USSR) **36**, 1918 (1959). Translated in: Soviet Phys. JETP **9**, 1364 (1959).

[12] G. Eilenberger. Z. Phys. **214**, 195 (1968).

[13] A. I. Larkin and Yu. N. Ovchinnikov, Sov. Phys. JETP **28**. 1200 (1969).

[14] J.G. Bednorz and K.A. Müller. Z. Phys. **64**, 189 (1986).

[15] L.N. Cooper. Phys. Rev. **104**, 1189 (1956).

[16] H. F. Hess. R. B. Robinson. and J. V. Waszczak. Phys. Rev. Lett. **62**, 214 (1989).

[17] H. F. Hess. R. B. Robinson. and J. V. Waszczak. Phys. Rev. Lett. **64**, 2711 (1990).

[18] H. F. Hess. R. B. Robinson. and J. V. Waszczak. Physica B **169**, 422 (1991).

[19] U. Klein. Phys. Rev. B **41**, 4819 (1990).

[20] F. Gygi and M. Schlüter. Phys. Rev. B **43**, 7609 (1991).

[21] F. Gygi and M. Schlüter, Phys. Rev. B **65**, 1820 (1990).

[22] N. Schopohl and K. Maki, Phys. Rev. B **52**, 490 (1995).

[23] N. Hayashi. M. Ichioka, and K. Machida, Phys. Rev. Lett. **77**, 4074 (1996).

[24] N. Hayashi. M. Ichioka, and K. Machida, Phys. Rev. B **56**, 9052 (1997).

[25] J.R. Schrieffer. *Theory of Superconductivity*. W.A. Benjamin Inc.. New York. 1964.

[26] C. G. Kuper. *An Introduction to the Theory of Superconductivity*. Clarendon Press. Oxford. 1968.

[27] E.V. Thuneberg. J. Kurkijärvi. and D. Rainer. Phys. Rev. B **29**, 3913 (1984).

[28] M. Ichioka. N. Hayashi. N. Enomoto. and K. Machida. Phys. Rev. B **53**, 15316 (1996).

[29] N. Schopohl. cond-mat/9804064.

[30] M. Franz and Z. Tešanović. Phys. Rev. Lett. **80**, 4763 (1998).

[31] M.Yu. Kuchiev. P.V. Shevchenko. and O.P. Sushkov. cond-mat/9706135.

[32] W.H. Press. S.A. Teukolsky. W.T. Vetterling. and B.P. Flannery. *Numerical Recipes in C. Second Edition*. Cambridge University Press. 1992.

[33] J. Stewart. *Calculus. Second Edition*. Brooks/Cole Publishing Company. California. 1987.

Appendix A

Riccati transformation

A derivation of the Riccati transformation method is found in Ref. [29]. Here, we simply show the algebra involved in decoupling the Eilenberger equations. Namely, we demonstrate how the parameterization of Schopohl and Maki[22]:

$$\bar{f} = \frac{2\bar{a}}{1 + \bar{a}\bar{b}}, \quad \bar{f}^{\dagger} = \frac{2\bar{b}}{1 + \bar{a}\bar{b}}, \quad g = \frac{1 - \bar{a}\bar{b}}{1 + \bar{a}\bar{b}} \tag{A.1}$$

decouples the Eilenberger equations:

$$\frac{dg}{dx} = \bar{\Delta}^{*}(x)\bar{f}(x) - \bar{\Delta}(x)\bar{f}^{\dagger}(x). \tag{A.2}$$

$$\left\{ \omega_n - \frac{1}{2}\left(\frac{d}{dx} + i\frac{r_\perp}{r^2} \right) \right\} \bar{f}^{\dagger}(x) = \bar{\Delta}^{*}(x)g(x). \tag{A.3}$$

$$\left\{ \omega_n + \frac{1}{2}\left(\frac{d}{dx} - i\frac{r_\perp}{r^2} \right) \right\} \bar{f}(x) = \bar{\Delta}(x)g(x). \tag{A.4}$$

into these two ordinary differential equations:

$$\frac{d}{dx}\bar{a}(x) = \bar{\Delta}(x) - \left\{ 2\omega_n - i\frac{r_\perp}{r^2} + \bar{\Delta}^{*}(x)\bar{a}(x) \right\} \bar{a}(x). \tag{A.5}$$

$$\frac{d}{dx}\bar{b}(x) = -\bar{\Delta}^{*}(x) + \left\{ 2\omega_n - i\frac{r_\perp}{r^2} + \bar{\Delta}(x)\bar{b}(x) \right\} \bar{b}(x). \tag{A.6}$$

We use the same coordinate system as described in Section §2.3 with $x \equiv \rho(u) \cdot \hat{\mathbf{u}} = u$.

44

A.1 Decoupling the Eilenberger equations

It is easily seen that the parameterization satisfies the normalization condition:

$$
\begin{aligned}
g^2 &= \frac{(1 - \bar{a}\bar{b})^2}{(1 + \bar{a}\bar{b})^2} \\
&= \frac{1 - 2\bar{a}\bar{b} + (\bar{a}\bar{b})^2}{(1 + \bar{a}\bar{b})^2} \\
&= \frac{1 + 2\bar{a}\bar{b} + (\bar{a}\bar{b})^2 - 4\bar{a}\bar{b}}{(1 + \bar{a}\bar{b})^2} \\
&= \frac{(1 + \bar{a}\bar{b})^2 - 4\bar{a}\bar{b}}{(1 + \bar{a}\bar{b})^2} \\
&= 1 - \left(\frac{2\bar{a}}{1 + \bar{a}\bar{b}}\right)\left(\frac{2\bar{b}}{1 + \bar{a}\bar{b}}\right) \\
&= 1 - \bar{f}\bar{f}^\dagger
\end{aligned}
\tag{A.7}
$$

Now, to illustrate the decoupling of the Eilenberger equations, (A.2) - (A.4), let us start by examining the derivative of g.

$$
\begin{aligned}
\frac{dg}{dx} &= \frac{d}{dx}\left(\frac{1 - \bar{a}\bar{b}}{1 + \bar{a}\bar{b}}\right) \\
&= \left(\frac{-1}{1 + \bar{a}\bar{b}}\right)\frac{d}{dx}(\bar{a}\bar{b}) - \left(\frac{1 - \bar{a}\bar{b}}{(1 + \bar{a}\bar{b})^2}\right)\frac{d}{dx}(\bar{a}\bar{b}) \\
&= \left(\frac{-2}{(1 + \bar{a}\bar{b})^2}\right)\frac{d}{dx}(\bar{a}\bar{b})
\end{aligned}
\tag{A.8}
$$

As it turns out, this expression for $\frac{dg}{dx}$ can be incorporated into $\frac{d\bar{f}}{dx}$:

$$
\begin{aligned}
\frac{d\bar{f}}{dx} &= \frac{d}{dx}\left(\frac{2\bar{a}}{1 + \bar{a}\bar{b}}\right) \\
&= \left(\frac{2}{1 + \bar{a}\bar{b}}\right)\frac{d\bar{a}}{dx} - \left(\frac{2\bar{a}}{(1 + \bar{a}\bar{b})^2}\right)\frac{d}{dx}(\bar{a}\bar{b}) \\
&= \left(\frac{2}{1 + \bar{a}\bar{b}}\right)\frac{d\bar{a}}{dx} + \bar{a}\frac{dg}{dx}
\end{aligned}
\tag{A.9}
$$

And using (A.2) for $\frac{dg}{dx}$ in the last term gives:

$$
\begin{aligned}
\frac{d\bar{f}}{dx} &= \left(\frac{2}{1 + \bar{a}\bar{b}}\right)\frac{d\bar{a}}{dx} + \bar{a}(\bar{\Delta}^*\bar{f} - \bar{\Delta}\bar{f}^\dagger) \\
&= \left(\frac{2}{1 + \bar{a}\bar{b}}\right)\left\{\frac{d\bar{a}}{dx} + \bar{\Delta}^*\bar{a}^2 - \bar{\Delta}\bar{a}\bar{b}\right\}
\end{aligned}
\tag{A.10}
$$

A similar calculation can be done for $\frac{d\bar{f}^\dagger}{dx}$:

$$\begin{aligned}
\frac{d\bar{f}^\dagger}{dx} &= \frac{d}{dx}\left(\frac{2\bar{b}}{1+\bar{a}\bar{b}}\right) \\
&= \left(\frac{2}{1+\bar{a}\bar{b}}\right)\frac{d\bar{b}}{dx} - \left(\frac{2\bar{b}}{(1+\bar{a}\bar{b})^2}\right)\frac{d}{dx}(\bar{a}\bar{b}) \\
&= \left(\frac{2}{1+\bar{a}\bar{b}}\right)\frac{d\bar{b}}{dx} + \bar{b}\frac{dg}{dx} \\
&= \left(\frac{2}{1+\bar{a}\bar{b}}\right)\frac{d\bar{b}}{dx} + \bar{b}(\bar{\Delta}^\cdot\bar{f} - \bar{\Delta}\bar{f}^\dagger) \\
&= \left(\frac{2}{1+\bar{a}\bar{b}}\right)\left\{\frac{d\bar{b}}{dx} + \bar{\Delta}^\cdot\bar{a}\bar{b} - \bar{\Delta}\bar{b}^2\right\}
\end{aligned}$$ (A.11)

Substituting (A.10) into (A.4) yields the Riccati equation for $\bar{a}$:

$$\left\{\omega_n + \frac{1}{2}(\frac{d}{dx} + i\partial_{\parallel}\varphi)\right\}\bar{f} = \bar{\Delta}g$$

$$\frac{d\bar{a}}{dx} + \bar{\Delta}^\cdot\bar{a}^2 - \bar{\Delta}\bar{a}\bar{b} + (\omega_n + \frac{1}{2}i\partial_{\parallel}\varphi)(2\bar{a}) = \bar{\Delta}(1 - \bar{a}\bar{b})$$

$$\frac{d\bar{a}}{dx} = \bar{\Delta} - \left\{2\omega_n + i\partial_{\parallel}\varphi + \bar{\Delta}^\cdot\bar{a}\right\}\bar{a}$$ (A.12)

And the equation for $\bar{b}$ is found using (A.11) and (A.3):

$$\left\{\omega_n - \frac{1}{2}(\frac{d}{dx} - i\partial_{\parallel}\varphi)\right\}\bar{f}^\dagger = \bar{\Delta}^\cdot g$$

$$-\frac{d\bar{b}}{dx} - \bar{\Delta}^\cdot\bar{a}\bar{b} + \bar{\Delta}\bar{b}^2 + (\omega_n + \frac{1}{2}i\partial_{\parallel}\varphi)(2\bar{b}) = \bar{\Delta}^\cdot(1 - \bar{a}\bar{b})$$

$$\frac{d\bar{b}}{dx} = -\bar{\Delta}^\cdot + \left\{2\omega_n + i\partial_{\parallel}\varphi + \bar{\Delta}^\cdot\bar{b}\right\}\bar{b}$$ (A.13)

46

Appendix B

Numerical Methods

B.1 First-order differential equations

For a first order differential equation. the initial value problem can be expressed in an explicit form as:

$$\frac{dy}{dx} = f(x. y).$$

$$y(x_0) = y_0.$$

(B.1)

The basic strategy for finding a numerical solution to (B.1) consists of approximating the derivative as a difference:

$$\frac{dy}{dx} \approx \frac{y_{n+1} - y_n}{x_{n+1} - x_n},$$

(B.2)

and then compute the next y value as one takes a step in the x direction:

$$y_{n+1} = y_n + hf(x_n, y_n).$$

(B.3)

where $h = x_{n+1} - x_n$. The solution advances through an interval h, but uses derivative information only at the beginning of the interval, resulting in an error term of $O(h^2)$. That is, (B.3) is just the power series expansion to first order.

B.1.1 Fourth-order Runge-Kutta Method

In general. the Runge-Kutta method achieves higher order accuracy by making a "trial" evaluation at the midpoint of the step interval. Then. the information found at the midpoint is used to compute the "real" step across the whole interval. The intermediate steps still produce a first order solution. yet give different coefficients of higher-order error terms. By adding up the right combination. error terms can be eliminated order by order.

The recipe for the fourth-order Runge-Kutta method is[32]:

$$
\begin{aligned}
k_1 &= hf(x_n. y_n). \\
k_2 &= hf(x_n + \frac{h}{2}. y_n + \frac{k_1}{2}). \\
k_3 &= hf(x_n + \frac{h}{2}. y_n + \frac{k_2}{2}). \\
k_4 &= hf(x_n + h. y_n + k_3). \\
y_{n+1} &= y_n + \frac{k_1}{6} + \frac{k_2}{3} + \frac{k_3}{3} + \frac{k_4}{6} + O(h^5).
\end{aligned}
\tag{B.4}
$$

B.1.2 Adaptive stepsize control

For performance reasons. it is beneficial to make frequent changes to the stepsize h. so that a solution may be found with minimal computational effort. In order to make such stepsize adjustments. the program must be capable of estimating the error during each iteration of the algorithm.

In our work. we adopt an embedded Runge-Kutta formula[32] to achieve adaptive stepsize control. The recipe consists of a fifth-order method from six function evaluations. where another combination of the six functions gives a fourth-order method. The difference between the two methods is used as an estimate of the truncation error. and thus provides a measure on how to adjust the stepsize.

48

The general form of the fifth-order Runge-Kutta formula is:

$$k_1 = hf(x_n. y_n).$$

$$k_2 = hf(x_n + a_2h. y_n + b_{21}k_1).$$

$$\dots$$

$$k_6 = hf(x_n + a_6h. y_n + b_{61}k_1 + \dots + b_{65}k_5).$$

$$y_{n+1} = y_n + c_1k_1 + c_2k_2 + c_3k_3 + c_4k_4 + c_5k_5 + c_6k_6 + O(h^6). \qquad (B.5)$$

The embedded fourth-order formula is:

$$y_{n+1}^* = y_n + c_1^*k_1 + c_2^*k_2 + c_3^*k_3 + c_4^*k_4 + c_5^*k_5 + c_6^*k_6 + O(h^5). \qquad (B.6)$$

and the error estimate is given by:

$$\Delta \equiv y_{n+1} - y_{n+1}^* = \sum_{i=1}^{6}(c_i - c_i^*)k_i. \qquad (B.7)$$

where the various coefficients (known as Cash-Karp parameters) are given in Table B.1.

In order to adjust the stepsize. we notice that Δ scales as h^5. If an error of Δ_1 results from a stepsize of h_1. we may then estimate a desired error of Δ_0 by taking a step given by h_0:

$$h_0 = h_1 \left| \frac{\Delta_0}{\Delta_1} \right|^{\frac{1}{5}}. \qquad (B.8)$$

Thus. if Δ_1 is larger in magnitude that Δ_0, then the error is greater than our desired accuracy and the step must be repeated. We try a shorter stepsize given by (B.8). Conversely. if Δ_1 is smaller than Δ_0. then (B.8) tells us how much we can increase the stepsize for the next iteration.

i	a_i	c_i	c_i^*
1		$\frac{37}{378}$	$\frac{2825}{27648}$
2	$\frac{1}{5}$	0	0
3	$\frac{3}{10}$	$\frac{250}{621}$	$\frac{18575}{48384}$
4	$\frac{3}{5}$	$\frac{125}{594}$	$\frac{13525}{55296}$
5	1	0	$\frac{277}{14336}$
6	$\frac{7}{8}$	$\frac{512}{1771}$	$\frac{1}{4}$

b_{ij}	$j=1$	2	3	4	5
$i=1$					
2	$\frac{1}{5}$				
3	$\frac{3}{40}$	$\frac{9}{40}$			
4	$\frac{3}{10}$	$\frac{-9}{10}$	$\frac{6}{5}$		
5	$\frac{-11}{54}$	$\frac{5}{2}$	$\frac{-70}{27}$	$\frac{35}{27}$	
6	$\frac{1631}{55296}$	$\frac{175}{512}$	$\frac{575}{13824}$	$\frac{44275}{110592}$	$\frac{253}{4096}$

Table B.1: Cash-Karp parameters for the embedded Runge-Kutta method.

B.2 Numerical integration using Simpson's rule

A definite integral:

$$S = \int_a^b f(x)dx \tag{B.9}$$

is solved numerically by approximating the integrand $f(x)$ by functions which can be easily integrated. Piecewise quadratic approximations result in Simpson's rule, which is a fourth-order method defined as[33]:

$$\int_a^b f(x)dx \approx \frac{\Delta x}{3}[f(x_0) + 4f(x_1) + 2f(x_2) + 4f(x_3) + \ldots$$
$$+ 2f(x_{n-2}) + 4f(x_{n-1}) + f(x_n)]. \tag{B.10}$$

where n is even and $\Delta x = (b-a)/n$. Note that this method is similar to the fourth-order Runge-Kutta method when $f(x, y)$ depends only on x.

Appendix C

Source code

C.1 Program listing

A set of C functions has been developed to solve the Eilenberger equations. The source code of these routines is shown here. along with a sample main() to illustrate the functionality.

```
#include <stdio.h>
#include <math.h>
#include <stdlib.h>
#include <time.h>
#include <stddef.h>

#include "rkutil.h"

#ifndef PI
#define PI          3.141592653589793
#endif

#define Kb          1.000
#define EPSILON     1e-8

/* DEFINITION STANDARD - FEB 26, 1998 */
#define DWAVE       1
#define SWAVE       2
#define NBSE2_5      3
#define NBSE2_3      4
```

```c
#define DPID_2     5
#define DPID_5     6
#define DPID_8     7
#define DPID_X     8
#define SPD_X      9
#define SPD_5      10
#define SPD_2      11
#define DPS_2      12
#define DPS_5      13
#define ABSD       14
#define DPIS_1     15
#define DPIS_2     16
#define DPIS_X     17

int     gSTATE = SWAVE;
double gTheta;
double gWR, gWI;
double gRperp;
double gToTc = 0.0;

FILE *logFILE;

typedef struct
        {
        double  x1;
        double  x2;
        double  inc;
        int     i1;
        int     i2;
        int     iinc;
        double  dfac;
        } LIMIT_TYPE;


double ANGFN_RE(double c)
        {
        switch (gSTATE)
                {
                case DPID_2:
                case DPID_5:
                case DPID_8:
                case DPID_X:
                case DPIS_1:
                case DPIS_2:
                case DPIS_X:
                case DWAVE:        return (cos(2*c)                );
```

```
                case SWAVE:        return (1.0                         );

                case NBSE2_5:      return (1.0+0.5*cos(6.0*c)         );
                case NBSE2_3:      return (1.0+cos(6.0*c)/3.0         );

                case SPD_X:        return (1.0+cos(2.0*c)            );
                case SPD_5:        return (1.0+0.5*cos(2.0*c)        );
                case SPD_2:        return (1.0+0.2*cos(2.0*c)        );

                case DPS_2:        return (cos(2.0*c)+0.2            );
                case DPS_5:        return (cos(2.0*c)+0.5            );

                case ABSD:         return (fabs(cos(2.0*c))          );
                }
        }

double ANGFN_IM(double c)
        {
        switch (gSTATE)
                {
                case DWAVE:
                case SWAVE:
                case NBSE2_5:
                case NBSE2_3:
                case SPD_X:
                case SPD_5:
                case SPD_2:
                case DPS_2:
                case DPS_5:
                case ABSD:         return (0.0                       );

                case DPID_2:       return (0.2*sin(2.0*c)    );
                case DPID_5:       return (0.5*sin(2.0*c)    );
                case DPID_8:       return (0.8*sin(2.0*c)    );
                case DPID_X:       return (sin(2.0*c)        );
                case DPIS_1:       return (0.1               );
                case DPIS_2:       return (0.2               );
                case DPIS_X:       return (1.0               );
                }
        }

double deltaT()
        {
        return(1.0);
        }

void calGreens(double y[], double ffg[])
```

53

```c
        {
        double a1,a2,b1,b2, denom;

        a1 = y[0];
        a2 = y[1];
        b1 = y[2];
        b2 = y[3];

        denom = 1+a1*a1*b1*b1 + a2*a2*b2*b2 - 2*a2*b2
                + 2*a1*b1 + a1*a1*b2*b2 + a2*a2*b1*b1;

        ffg[0]=(2*a1 + 2*a1*a1*b1 + 2*a2*a2*b1) / denom ;
        ffg[1]=(-2*a1*a1*b2 - 2*a2*a2*b2 + 2*a2) / denom;
        ffg[2]=(2*b1 + 2*a1*b1*b1 + 2*a1*b2*b2) / denom ;
        ffg[3]=(-2*a2*b1*b1 - 2*a2*b2*b2 + 2*b2) / denom;
        ffg[4]=(1-a2*a2*b1*b1-a1*a1*b2*b2-a1*a1*b1*b1-a2*a2*b2*b2)/denom;
        ffg[5]=(-2*a2*b1 - 2*a1*b2)/denom;
        return;
        }

void fa(double x, double y[], double dydx[])
        {
        double DR, DI, AR, AI, DRR, DRI, TR, TI;
        double CB1R, CB1I;
        double r;

        r = sqrt(x*x + gRperp*gRperp);

        AR = y[0];                              /* FIRST CHANNEL = AR */
        AI = y[1];                              /* SECOND CHANNEL = AI */

        DRR = deltaT() * tanh(r);               /* DELTA(r) */
        DRI = 0.0;

        TR = ANGFN_RE(gTheta);                  /* F(theta) */
        TI = ANGFN_IM(gTheta);

        DR = DRR*TR - DRI*TI;                    /* DELTA(r,theta) */
        DI = DRR*TI + DRI*TR;

        CB1R = 2*gWR + DR*AR + DI*AI;
        CB1I = 2*gWI -gRperp/(r*r) - DI*AR + DR*AI;

        dydx[0] =  DR - CB1R*AR + CB1I*AI;
        dydx[1] =  DI - CB1R*AI - CB1I*AR;
        return;
        }
```

54

```c
void fb(double x, double y[], double dydx[])
        {
        double DR, DI, BR, BI, DRR, DRI, TR, TI;
        double CB2R, CB2I;
        double r;

        r = sqrt(x*x + gRperp*gRperp);

        BR = y[0];                              /* THIRD CHANNEL = BR */
        BI = y[1];                              /* FOURTH CHANNEL = BI */

        DRR = deltaT() * tanh(r);               /* DELTA(r) */
        DRI = 0.0;

        TR = ANGFN_RE(gTheta);                  /* F(theta) */
        TI = ANGFN_IM(gTheta);

        DR = DRR*TR - DRI*TI;                    /* DELTA(r,theta) */
        DI = DRR*TI + DRI*TR;

        CB2R = 2*gWR + DR*BR - DI*BI;
        CB2I = 2*gWI -gRperp/(r*r) + DR*BI - DI*BR;

        dydx[0] = -DR + CB2R*BR - CB2I*BI;
        dydx[1] =  DI + CB2R*BI + CB2I*BR;
        return;
        }

void faOPT(double x, double y[], double dydx[])
        {
        double DR, DI, AR, AI, DRR, DRI, TR, TI;
        double CB1R, CB1I;
        double r;

        r = sqrt(x*x + gRperp*gRperp);

        AR = y[0];                              /* FIRST CHANNEL = AR */
        AI = y[1];                              /* SECOND CHANNEL = AI */

        DRR = deltaT() * tanh(r);               /* DELTA(r) */
        DRI = 0.0;

        TR = ANGFN_RE(gTheta);                  /* F(theta) */
        TI = ANGFN_IM(gTheta);

        DR = DRR*TR - DRI*TI;                    /* DELTA(r,theta) */
```

```
              DI = DRR*TI + DRI*TR;

              CB1R = 2*gWR + DR*AR + DI*AI;
              CB1I = 2*gWI - DI*AR + DR*AI;

              dydx[0] =  DR - CB1R*AR + CB1I*AI;
              dydx[1] =  DI - CB1R*AI - CB1I*AR;
              return;
              }

void fbOPT(double x, double y[], double dydx[])
              {
              double DR, DI, BR, BI, DRR, DRI, TR, TI;
              double CB2R, CB2I;
              double r;

              r = sqrt(x*x + gRperp*gRperp);

              BR = y[0];                        /* THIRD CHANNEL = BR */
              BI = y[1];                        /* FOURTH CHANNEL = BI */

              DRR = deltaT() * tanh(r);         /* DELTA(r) */
              DRI = 0.0;

              TR = ANGFN_RE(gTheta);            /* F(theta) */
              TI = ANGFN_IM(gTheta);

              DR = DRR*TR - DRI*TI;             /* DELTA(r,theta) */
              DI = DRR*TI + DRI*TR;

              CB2R = 2*gWR + DR*BR - DI*BI;
              CB2I = 2*gWI + DR*BI - DI*BR;

              dydx[0] = -DR + CB2R*BR - CB2I*BI;
              dydx[1] =  DI + CB2R*BI + CB2I*BR;
              return;
              }

double gFromAB(double rpar, double rperp, double theta, double E, double n)
              {
              double rparPlimit, rparNlimit;
              double DRR, DRI, DR, DI, TR, TI, WR, WI;
              double ivdm2, ivx, ivy, ivr, ivtheta, ivp, ivq;
              double y[2], yAB[4], ffg[6], aRe, aIm, bRe, bIm;
              double realInt;
              int Tindex;
```

```c
        double hstart, eps, hmin;
        int kount, inNok, inNbad, exNok, exNbad;

        eps = 1.0e-4;
        hstart = 0.01;
        hmin = eps*1.0e-7;

        exNok = 0;
        exNbad = 0;
        rparPlimit = 10;
        rparNlimit = -10;
        WR = n;
        WI = -E;

/* SET GLOBALS */
        gTheta = theta;
        gRperp = rperp;
        gWR = WR;
        gWI = WI;

/* POSITIVE INITIAL VALUE (B-CHANNEL) */
        DRR = deltaT()*tanh(sqrt(rparPlimit*rparPlimit+rperp*rperp));
        DRI = 0.0;                              /* DELTA(r) */

        TR = ANGFN_RE(gTheta);                  /* F(theta) */
        TI = ANGFN_IM(gTheta);

        DR = DRR*TR - DRI*TI;                   /* DELTA(r,theta) */
        DI = DRR*TI + DRI*TR;

        ivdm2 = DR*DR + DI*DI;

        if (ivdm2 == 0.0)
                {
                y[0] = 0.0;
                y[1] = 0.0;
                }
        else
                {

                ivx = WR*WR - WI*WI + ivdm2;
                ivy = 2*WR*WI;

                if ((ivx >= 0) && (ivy >= 0))
                        ivtheta = atan(ivy/ivx);
                else if ((ivx < 0) && (ivy >= 0))
                        ivtheta = atan(ivy/ivx) + PI;
```

57

```
            else if ((ivx < 0) && (ivy < 0))
                    ivtheta = atan(ivy/ivx) + PI;
            else if ((ivx >= 0) && (ivy < 0))
                    ivtheta = atan(ivy/ivx) + 2*PI;

            ivr = sqrt(ivx*ivx + ivy*ivy);

            if (cos(ivtheta/2.0) < 0)
                    {
                    ivp = -sqrt(ivr)*cos(ivtheta/2.0) - WR;
                    ivq = -sqrt(ivr)*sin(ivtheta/2.0) - WI;
                    }
            else
                    {
                    ivp = sqrt(ivr)*cos(ivtheta/2.0) - WR;
                    ivq = sqrt(ivr)*sin(ivtheta/2.0) - WI;
                    }

            y[0] = ( ivp*DR + ivq*DI) / ivdm2;
            y[1] = (-ivp*DI + ivq*DR) / ivdm2;


            }
    if (fabs(gRperp) < EPSILON)
            kount  = odeint(y, 2, rparPlimit, rpar, eps,
                            hstart, hmin, &inNok, &inNbad, fbOPT);
    else
            kount  = odeint(y, 2, rparPlimit, rpar, eps,
                            hstart, hmin, &inNok, &inNbad, fb);

    yAB[2] = y[0];
    yAB[3] = y[1];


/* NEGATIVE INITIAL VALUE (A-CHANNEL) */
    DRR = deltaT() * tanh(sqrt(rparNlimit*rparNlimit + rperp*rperp));
    DRI = 0.0;                         /* DELTA(r) */

    TR = ANGFN_RE(gTheta);             /* F(theta) */
    TI = ANGFN_IM(gTheta);

    DR = DRR*TR - DRI*TI;              /* DELTA(r,theta) */
    DI = DRR*TI + DRI*TR;

    ivdm2 = DR*DR + DI*DI;

    if (ivdm2 == 0.0)
            {
```

```
        y[0] = 0.0;
        y[1] = 0.0;
        }
else
        {

        ivx = WR*WR - WI*WI + ivdm2;
        ivy = 2*WR*WI;

        if ((ivx >= 0) && (ivy >= 0))
                ivtheta = atan(ivy/ivx);
        else if ((ivx < 0) && (ivy >= 0))
                ivtheta = atan(ivy/ivx) + PI;
        else if ((ivx < 0) && (ivy < 0))
                ivtheta = atan(ivy/ivx) + PI;
        else if ((ivx >= 0) && (ivy < 0))
                ivtheta = atan(ivy/ivx) + 2*PI;

        ivr = sqrt(ivx*ivx + ivy*ivy);

        if (cos(ivtheta/2.0) < 0)
                {
                ivp = -sqrt(ivr)*cos(ivtheta/2.0) - WR;
                ivq = -sqrt(ivr)*sin(ivtheta/2.0) - WI;
                }
        else
                {
                ivp = sqrt(ivr)*cos(ivtheta/2.0) - WR;
                ivq = sqrt(ivr)*sin(ivtheta/2.0) - WI;
                }

        y[0] = ( ivp*DR - ivq*DI) / ivdm2;
        y[1] = ( ivp*DI + ivq*DR) / ivdm2;
        }
if (fabs(gRperp) < EPSILON)
        kount += odeint(y, 2, rparNlimit, rpar, eps,
                        hstart, hmin, &inNok,&inNbad,faOPT);
else
        kount += odeint(y, 2, rparNlimit, rpar, eps,
                        hstart, hmin, &inNok, &inNbad, fa);


yAB[0] = y[0];
yAB[1] = y[1];

calGreens(yAB, ffg);
return (ffg[4]);
}
```

```c
double gFromABxy(double xyX, double xyY, double theta, double E, double n)
        {
        double rpar, rperp;

        rpar = xyX*cos(theta) + xyY*sin(theta);
        rperp = -xyX*sin(theta) + xyY*cos(theta);

        return ( gFromAB(rpar,rperp,theta,E,n) );
        }

void gVsTheta(double xyX, double xyY, LIMIT_TYPE t, double E,
        double n, char *filename)
        {
        FILE *stream;
        int i;
        double theta;

        stream = fopen(filename, "wt");

        for (theta = t.x1; theta <= t.x2; theta += t.inc)
                fprintf (stream,
                        "%10.6f%10.6f\n",
                        theta, gFromABxy(xyX, xyY, theta, E, n) );
        fclose(stream);
        }

void gVsRpar(LIMIT_TYPE r, double rperp, double theta, double E,
        double n, char *filename)
        {
        FILE *stream;
        int i;
        double rpar;

        stream = fopen(filename, "wt");

        for (rpar = r.x1; rpar <= r.x2; rpar += r.inc)
                fprintf (stream,
                        "%10.6f%10.6f\n",
                        rpar, gFromAB(rpar, rperp, theta, E, n) );
        fclose(stream);
        }

void gVsRperp(double rpar, LIMIT_TYPE r, double theta, double E,
        double n, char *filename)
        {
        FILE *stream;
```

```c
        int i;
        double rperp;

        stream = fopen(filename, "wt");

        for (rperp = r.x1; rperp <= r.x2; rperp += r.inc)
                fprintf (stream,
                        "%10.6f%10.6f\n",
                        rperp, gFromAB(rpar, rperp, theta, E, n) );
        fclose(stream);
        }

void rVsLDOSyline(LIMIT_TYPE x, double xyY, double E,
        double n, char *filename)
        {
        FILE *stream;
        int i, thetaPoints, fixer, scount;
        double r, xyX, theta, realInt;
        double *integrand;
        double *store;
        double thetaMLX;

        thetaPoints = 1001;             /* MUST BE ODD FOR SIMPSON INT */
        thetaMLX = 0.006283;            /* USE MULTX SINCE LINUX CAN'T ADD */
        integrand = allocdv(thetaPoints);

        stream = fopen(filename, "wt");

        /* FIRST COUNT UP POINTS */
        /* MAR 7, FIXER ADDED TO FIX LINUX PRECISION PROBLEM */
        scount = 0;
        for (fixer = x.i1; fixer <= x.i2; fixer+= x.iinc)
                scount++;
        store = allocdv(scount);

        /* NOW EVALUATE POINTS */
        scount = 0;
        for (fixer = x.i1; fixer <= x.i2; fixer+= x.iinc)
                {
                xyX = x.dfac*(double)fixer;

                r = sqrt(xyX*xyX + xyY*xyY);

                if (r < EPSILON)        /* DISPLACE ORIGIN POINT */
                        xyX = 10*EPSILON;

                /* CALCULATE g VS theta */
```

61

```
                        for (i = 0; i < thetaPoints; i+= 1)
                                {
                                theta = (double)i*thetaMLX;
                                integrand[i] = gFromABxy (xyX, xyY, theta, E, n);
                                }

                        realInt = 0;                            /* INTEGRATE OVER theta */
                        simpsonInt(integrand, thetaPoints-1, 0, 2*PI, &realInt);

                        store[scount++] = realInt/(2*PI);
                        }

        /* AND WRITE OUT */
        scount = 0;
        for (fixer = x.i1; fixer <= x.i2; fixer += x.iinc)
                fprintf (stream,
                        "%8.4f%10.6f\n",
                        x.dfac*(double)fixer, store[scount++]);
        freedv(integrand);
        freedv(store);
        fclose(stream);
        }


void rVsLDOSphi(LIMIT_TYPE x, double phi, double E,
        double n, char *filename)
        {
        FILE *stream;
        int i, thetaPoints;
        double r, xyX, xyY, theta, realInt;
        double *integrand;
        double thetaMLX;

        thetaPoints = 1001;             /* MUST BE ODD FOR SIMPSON INT */
        thetaMLX = 0.006283;            /* USE MULTX SINCE LINUX CAN'T ADD */
        integrand = allocdv(thetaPoints);

        stream = fopen(filename, "wt");

        for (r = x.x1; r <= x.x2; r += x.inc)
                {
                if (r < EPSILON)
                        r = 10*EPSILON;

                xyX = r*cos(phi);
                xyY = r*sin(phi);
```

```c
        /* CALCULATE g VS theta */
        for (i = 0; i < thetaPoints; i+= 1)
            {
            theta = (double)i*thetaMLX;
            integrand[i] = gFromABxy (xyX, xyY, theta, E, n);
            }

        realInt = 0;                          /* INTEGRATE OVER theta */
        simpsonInt(integrand, thetaPoints-1, 0, 2*PI, &realInt);

        fprintf (stream,
            "%8.4f%10.6f\n",
            sqrt(xyX*xyX+xyY*xyY), realInt/(2*PI) );

        }

    freedv(integrand);
    fclose(stream);
    }

void eVsLDOSphi(double r, double phi, LIMIT_TYPE x,
        double n, char *filename)
    {
    FILE *stream;
    int i, thetaPoints;
    double xyX, xyY, theta, realInt, E;
    double thetaMLX;
    double *integrand;

    thetaPoints = 1001;                  /* MUST BE ODD FOR SIMPSON INT */
    thetaMLX = 0.006283;                 /* USE MULTX SINCE LINUX CAN'T ADD */
    integrand = allocdv(thetaPoints);

    stream = fopen(filename, "wt");

    for (E = x.x1; E <= x.x2; E += x.inc)
        {
        if (r < EPSILON)
            r = 10*EPSILON;

        xyX = r*cos(phi);
        xyY = r*sin(phi);

        /* CALCULATE g VS theta */
        for (i = 0; i < thetaPoints; i+= 1)
            {
            theta = (double)i*thetaMLX;
            integrand[i] = gFromABxy (xyX, xyY, theta, E, n);
            }
```

```
                realInt = 0;                        /* INTEGRATE OVER theta */
                simpsonInt(integrand, thetaPoints-1, 0, 2*PI, &realInt);

                fprintf (stream, "%8.4f%10.6f\n", E, realInt/(2*PI) );
                }

        freedv(integrand);
        fclose(stream);
        }


char *thetime()
        {
        time_t t;
        t = time(0);
        return(ctime((time_t *)&t));
        }


void main(int argc, char *argv[])
        {
        int y, i, r;
        char string[80];
        LIMIT_TYPE x;
        double n, Eval, phiVal;
        char IDSTR[4], ESTR[4], PSTR[4];
        char DIREC[32];
        char exCommand[80];


        n = 0.03;                      /* ETA */


        /* SET MAP RANGE */
        x.x1 = 0.0;         x.x2 = 1.0;          x.inc = 0.02;


        /* MAKE ROOT DIRECTORY */
        gSTATE = DWAVE;          sprintf (IDSTR, "DX");
        sprintf (exCommand, "mkdir %s", IDSTR);
        system(exCommand);


        /* MAKE DIRECTORY FOR PHI DIRECTION */
        phiVal = 0.0;            sprintf (PSTR, "00");
        sprintf (DIREC, "%s/P%s", IDSTR, PSTR);
        sprintf (exCommand, "mkdir %s", DIREC);
        system(exCommand);


        /* CALCULATE MAP */
        for (r = 0; r < 301; r += 2)
                {
```

```
                sprintf (string,"%s/%s%sR%03d.DAT",DIREC,IDSTR,PSTR,r);
                eVsLDOSphi((double)r*0.01, phiVal, x, n, string);
                }


/* AND REPEAT FOR DIFFERENT phiVal */
gSTATE = DWAVE;            sprintf (IDSTR, "DX");
phiVal = PI/12.0;          sprintf (PSTR,  "15");
sprintf (DIREC, "%s/P%s", IDSTR, PSTR);
sprintf (exCommand, "mkdir %s", DIREC);
system(exCommand);


for (r = 0; r < 301; r += 2)
        {
        sprintf (string,"%s/%s%sR%03d.DAT",DIREC,IDSTR,PSTR,r);
        eVsLDOSphi((double)r*0.01, phiVal, x, n, string);
        }


/* AND AGAIN ... */
gSTATE = DWAVE;            sprintf (IDSTR, "DX");
phiVal = PI/4.0;           sprintf (PSTR,  "45");
sprintf (DIREC, "%s/P%s", IDSTR, PSTR);
sprintf (exCommand, "mkdir %s", DIREC);
system(exCommand);


for (r = 0; r < 301; r += 2)
        {
        sprintf (string,"%s/%s%sR%03d.DAT",DIREC,IDSTR,PSTR,r);
        eVsLDOSphi((double)r*0.01, phiVal, x, n, string);
        }
}
```
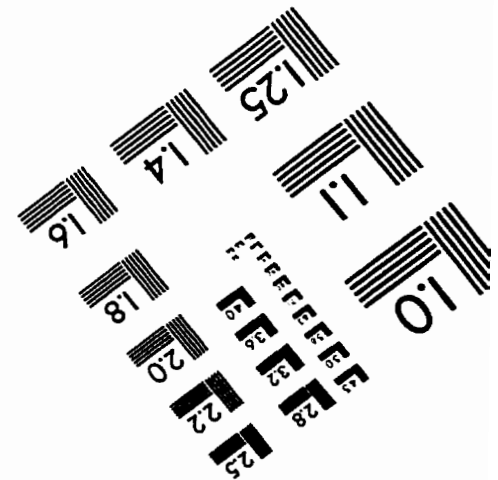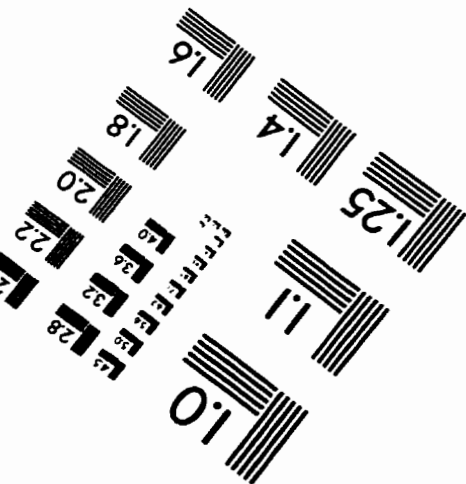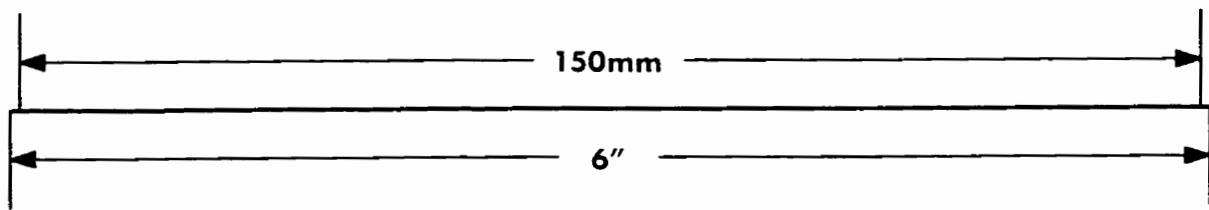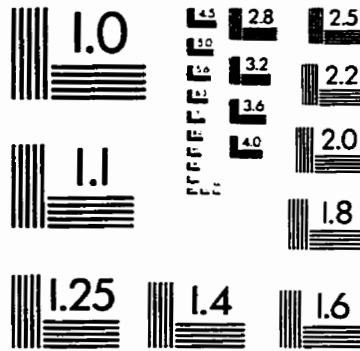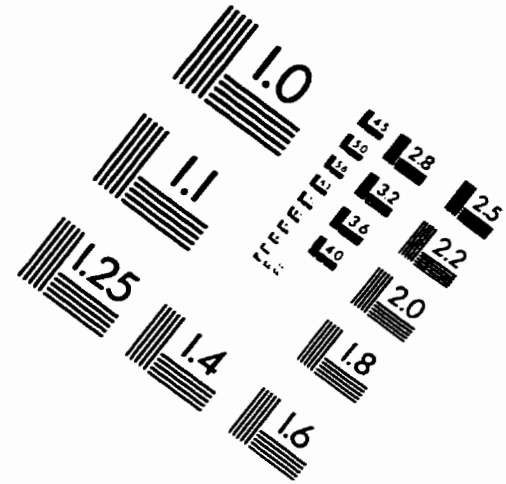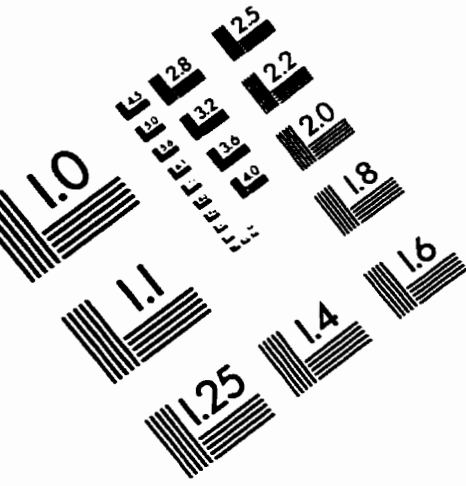
IMAGE EVALUATION
TEST TARGET (QA-3)

150mm

6"